THE JOURNAL OF BIOLOGICAL CHEMISTRY VOL. 287, NO. 45, pp. 37594–37609, November 2, 2012

Distinct Activation Properties of the Nuclear Factor of Activated T-cells (NFAT) Isoforms NFATc3 and NFATc4 in Neurons*[S]◆

Received for publication, March 21, 2012, and in revised form, September 7, 2012 Published, JBC Papers in Press, September 12, 2012, DOI 10.1074/jbc.M112.365197

Jason D. Ulrich[‡], Man-Su Kim[‡§], Patrick R. Houlihan[‡], Leonid P. Shutov[‡], Durga P. Mohapatra[‡], Stefan Strack[‡], and Yuriy M. Usachev[‡1]

From the [‡]Department of Pharmacology, University of Iowa Carver College of Medicine, Iowa City, Iowa 52242 and the [§]College of Pharmacy, Inje University, Gimhae, Republic of Korea

Background: Ca^{2+}/calcineurin-dependent transcription factor NFAT regulates many neuronal functions.
Results: Depolarization/Ca^{2+} influx-induced activation and nuclear translocation are markedly faster and stronger for NFATc3 than NFATc4 in neurons, which is determined in part by SP-containing regions of NFATc3 and NFATc4.
Conclusion: Activation of NFATc3 and NFATc4 is distinctly regulated in neurons.
Significance: The distinct regulation of NFATc3 and NFATc4 may underlie isoform-specific NFAT functions in neurons.

The Ca^{2+}/calcineurin-dependent transcription factor NFAT (nuclear factor of activated T-cells) is implicated in regulating dendritic and axonal development, synaptogenesis, and neuronal survival. Despite the increasing appreciation for the importance of NFAT-dependent transcription in the nervous system, the regulation and function of specific NFAT isoforms in neurons are poorly understood. Here, we compare the activation of NFATc3 and NFATc4 in hippocampal and dorsal root ganglion neurons following electrically evoked elevations of intracellular Ca^{2+} concentration ($[Ca^{2+}]_i$). We find that NFATc3 undergoes rapid dephosphorylation and nuclear translocation that are essentially complete within 20 min, although NFATc4 remains phosphorylated and localized to the cytosol, only exhibiting nuclear localization following prolonged (1–3 h) depolarization. Knocking down NFATc3, but not NFATc4, strongly diminished NFAT-mediated transcription induced by mild depolarization in neurons. By analyzing NFATc3/NFATc4 chimeras, we find that the region containing the serine-rich region-1 (SRR1) mildly affects initial NFAT translocation, although the region containing the serine-proline repeats is critical for determining the magnitude of NFAT activation and nuclear localization upon depolarization. Knockdown of glycogen synthase kinase 3β (GSK3β) significantly increased the depolarization-induced nuclear localization of NFATc4. In contrast, inhibition of p38 or mammalian target of rapamycin (mTOR) kinases had no significant effect on nuclear import of NFATc4. Thus, electrically evoked $[Ca^{2+}]_i$ elevation in neurons rapidly and strongly activates NFATc3, whereas activation of NFATc4 requires a coincident increase in $[Ca^{2+}]_i$ and suppression of GSK3β, with differences in the serine-proline-containing region giving rise to these distinct activation properties of NFATc3 and NFATc4.

Activity-dependent gene regulation enables cells to make durable adaptations in response to signaling experiences. Neurons couple electrical activity to elevations in intracellular calcium ($[Ca^{2+}]_i$)[2] through voltage-gated calcium channels (VGCCs) (1). Ca^{2+} influx through L-type VGCCs is especially critical for excitation-dependent gene transcription underlying important functions such as synaptic plasticity (2). Among the transcription factors activated by Ca^{2+} influx through L-type VGCC are the nuclear factor of activated T-cells (NFAT) family of proteins, which are activated by the Ca^{2+}/calmodulin (CaM)-dependent protein phosphatase, calcineurin (CaN) (3–6). NFAT proteins were first discovered as regulators of IL-2 expression in response to antigen receptor activation in T-cells (7–9). Subsequent studies identified four Ca^{2+}/CaN-dependent NFAT isoforms, denoted NFATc1–c4 and found that NFAT proteins were expressed in virtually all cell types (10, 11). NFAT-dependent gene regulation is important in the development and function of the immune, cardiovascular, and nervous systems (11–19). In the nervous system, NFAT activity regulates neurite outgrowth, synaptogenesis, neuronal development, and survival (20–27). Despite the critical role of NFAT-dependent transcription in neurons, little is known about the respective functions and regulation of specific NFAT isoforms.

NFAT proteins contain two major conserved regions as follows: a regulatory domain termed the NFAT-homology region (NHR) in the N-terminal portion of the protein and a Rel-homology DNA binding domain in the C-terminal portion of the

* This work was supported, in whole or in part, by National Institutes of Health Grants NS054614 and NS072432 (to Y. M. U.), NS043254 and NS056244 (to S. S.), NS069898 (to D. P. M.), and F31 MH081420 from NRSA (to J. D. U.).
◆ This article was selected as a Paper of the Week.
[S] This article contains supplemental Figs. 1 and 2 and Movies 1 and 2.
[1] To whom correspondence should be addressed: Dept. of Pharmacology, University of Iowa Carver College of Medicine, 2-250 BSB, 51 Newton Rd., Iowa City, IA 52242. Tel.: 319-335-9388; Fax: 319-335-8930; E-mail: yuriy-usachev@uiowa.edu.

[2] The abbreviations used are: $[Ca^{2+}]_i$, intracellular calcium; CaN, calcineurin; NFAT, nuclear factor of activated T-cells; DRG, dorsal root ganglion; VGCC, voltage-gated calcium channel; DIV, days *in vitro*; HS, horse serum; EGFP, enhanced GFP; LMB, leptomycin B; ANOVA, analysis of variance; SP, serine-proline; NLS, nuclear localization sequence; NHR, NFAT-homology region; mTOR, mammalian target of rapamycin.

protein (13, 28, 29). The NHR contains two CaN-binding motifs, a Ca^{2+}-independent P*X*I*X*IT motif in the N terminus and a Ca^{2+}-dependent L*X*VP motif in the C-terminal portion of NHR (30–32). Under basal conditions, the NHR is heavily phosphorylated on serine residues located within a serine-rich region (SRR1) and at a series of serine-proline (SP) motifs. Phosphorylation of the NHR is thought to occlude a nuclear localization sequence (NLS) within the NHR, resulting in cytosolic retention of NFAT under resting conditions. Elevations in $[Ca^{2+}]_i$ lead to activation of the Ca^{2+}/CaM-dependent protein phosphatase CaN, which then dephosphorylates NFAT, revealing the NLS and resulting in NFAT translocation to the nucleus.

CaN-mediated NFAT dephosphorylation is opposed by the activity of several kinases that either maintain NFAT phosphorylation within the cytosol to oppose nuclear import or rephosphorylate NFAT within the nucleus to facilitate nuclear export. Several protein kinases, including casein kinase 1 (CK1), c-Jun N-terminal kinase (JNK), p38, and mTOR kinases, phosphorylate SRR1, which is thought to be critical for maintaining the cytosolic localization of NFAT under resting conditions (33–37). GSK3β phosphorylates the SP motifs within NFAT (5, 38). GSK3β requires a priming phosphorylation on the substrate for enzymatic activity. DYRK1A, DYRK2, and PKA have all been shown to phosphorylate the SP motifs and facilitate NFAT phosphorylation by GSK3β (39–41).

Despite the shared activation by CaN-dependent dephosphorylation, the activity of specific NFAT isoforms within a single cell can be repressed through poorly understood mechanisms (42–44). Here, we describe the differential regulation of the two most commonly studied NFAT isoforms in neurons, NFATc3 and NFATc4 (5, 6, 20, 21, 23, 45–51). We find that although NFATc3 is rapidly dephosphorylated and translocates to the nucleus upon depolarization, NFATc4 remains phosphorylated and localized to the cytosol. Using chimeras of NFATc3 and NFATc4, we found that the N- and C-terminal halves of the NHR differentially affect NFATc4 nuclear translocation and retention upon prolonged $[Ca^{2+}]_i$ elevation. Furthermore, inhibition of NFATc4 nuclear localization was strongly dependent upon the basal activity of endogenous GSK3β.

EXPERIMENTAL PROCEDURES

Cell Culture—Primary DRG neuron cultures were prepared from P0–P2 Sprague-Dawley rat pups (Charles River Laboratories). Lumbar, thoracic, and cervical DRGs were removed and digested for 7 min at 37 °C with 1 mg/ml Pronase E (Serva Electrophoresis GmbH, Heidelberg, Germany) in DMEM/HEPES (20 mM, pH 7.4). Cells were then washed with DMEM/HEPES (20 mM, pH 7.4) followed by dissociation via trituration using fire-polished Pasteur pipettes. Dissociated cells were then plated onto the center of 25-mm glass coverslips coated with poly-L-ornithine (0.2 mg/ml in 150 mM boric acid buffer) and laminin (0.5 mg/ml in PBS, Roche Diagnostics). Cells were maintained in Complete DMEM containing 5% heat-inactivated horse serum (HS), 5% fetal bovine serum (FBS), 25 ng/ml nerve growth factor (NGF), penicillin (50 units/ml), and streptomycin (50 μg/ml) in a 10% CO_2 incubator at 37 °C. Cells were used 1–3 days after plating.

Hippocampal neurons were prepared from P0–P1 Sprague-Dawley rats (Charles River Laboratories, Wilmington, MA). Hippocampi were dissected in Hanks' buffered saline solution (Invitrogen) and digested with 0.3% trypsin for 9 min at 37 °C. Hippocampi were then washed in Hanks' buffered saline solution before dissociation via trituration. Cells were then counted and plated onto the center of 25-mm glass coverslips coated with poly-L-ornithine and laminin. Cells were incubated for 3–4 h in neurobasal A (Invitrogen) containing B27 (Invitrogen), 0.5 mM glutamine, 10 mM HEPES, and 5% HS. Media were then replaced with serum-free medium, and the cells were maintained in a 5% CO_2 incubator at 37 °C. One-third of the media volume was replaced once a week.

PC12 cells (PC6-3 subline (52)) were plated on rat tail collagen type I (BD Biosciences)-coated 6-well plates. Cells were maintained in RPMI 1640 medium containing 10% HS and 5% FBS in a 5% CO_2 incubator at 37 °C.

Transfection Protocols—Prior to plating, DRG neurons were transfected using the Amaxa nucleofection system (Lonza). DRGs from 4 to 5 pups were used for each transfection. Following trituration, cells were centrifuged at 80 × *g* for 5 min, resuspended in the rat neuron nucleofection solution (Lonza, VPG-1003), and mixed with the plasmid DNA. Cells were electroporated using program G-013 on a Nucleofector device (Lonza) followed by a 5-min recovery in complete DMEM at 37 °C. Cells were then plated and maintained as described above. Primary hippocampal neurons (7 DIV) and PC12 cells were transfected using Lipofectamine 2000 (Invitrogen) according to the manufacturer's protocol.

Expression Constructs—EGFP-NFATc4 was obtained from Addgene, Inc. (plasmid 10961; full-length human NFATc4, a gift from Dr. J. D. Molkentin to Addgene, Cambridge, MA) (53). EGFP-NFATc3 was generated by ligating full-length human NFATc3 (gift from Dr. Iino, the Tokyo Metropolitan Institute of Medical Science) (54) into pEGFP-C1 (Clontech). Hemagglutinin-tagged NFATc4 (HA-NFATc4), NFATc3-shRNA, NFATc4-shRNA, and GSK3β-shRNA were generous gifts from Dr. Hetman (University of Kentucky), whose group has described previously and validated these constructs (21). We have additionally confirmed efficacy of these shRNA constructs (supplemental Fig. 1). EGFP-NFATc4-R117Q, EGFP-NFATc3-Q112R, EGFP-NFATc4-VIVIT, EGFP-NFATc3-DQFLS, and EGFP-NFATc4-MDYLA were generated by site-directed mutagenesis using the QuikChange protocol (Stratagene). NFAT chimeras were generated by incorporating NotI and AscI restriction sites into NFATc3 and NFATc4 to allow for modular substitution of homologous regions. A NotI restriction site was incorporated into NFATc3 and NFATc4 through silent mutations in nucleotides encoding A200 and A206, respectively. Incorporation of an AscI restriction site into NFATc3 resulted in mutations of S402G, K403A, and K405W. Incorporation of an AscI restriction site into NFATc4 resulted in a mutation of I391P. Primers used to amplify fragments of NFATc3 and NFATc4 from EGFP-C1-NFATc3 or EGFP-C1-NFATc4 are indicated in Table 1. Following restriction digest, fragments were ligated into pEGFP-C1 using the rapid DNA

TABLE 1
Primers used to generate NFATc3-NFATc4 chimeras

Fragment	Fragment ID	Primers
EGFP-NFATc3(1–200)	NFAT c3-X-X	Forward: GTGAACCGTCAGATCCGCTAGC Reverse: ATTGCGGCCGCTTCATTCAACTCTGAGTCCAC
EGFP-NFATc4(1–206)	NFAT c4-X-X	Forward: GTGAACCGTCAGATCCGCTAGC Reverse: ATTGCGGCCGCCTCATTTAGCTCAGACTCCACC
EGFP-NFATc3(1–403)	NFAT c3-c3-X	Forward: GTGAACCGTCAGATCCGCTAGC Reverse: TAAGGCGCGCCTTGCTCCAGGTAAAGGGTGAAGG
EGFP-NFATc4(1–388)	NFAT c4-c4-X	Forward: GTGAACCGTCAGATCCGCTAGC Reverse: TTAGGCGCGCCTTGGACCAAGCGAGTGGG
NFATc3 (201–1075)	NFAT X-c3-c3	Forward: TAAGCGGCCGCCCGATTTACCCTTGGATCC Reverse: GTTTGGACAAACCACAACTAGAATGC
NFATc4 (207–902)	NFAT X-c4-c4	Forward: TAAGCGGCCGCCCGCTTTGGCCTGGGCTCC Reverse: GTTTGGACAAACCACAACTAGAATGC
NFATc3(404–1075)	NFAT X-X-c3	Forward: TAAGGCGCGCCCTGGCCACACCCCTATATTTCG Reverse: GTTTGGACAAACCACAACTAGAATGC
NFATc4(389–902)	NFAT X-X-c4	Forward: ATTGGCGCGCCCTGGGGGACACAGCCCTATCTTC Reverse: GTTTGGACAAACCACAACTAGAATGC
NFATc3(201–403)	NFAT X-c3-X	Forward: TAAGCGGCCGCCCGATTTACCCTTGGATCC Reverse: TAAGGCGCGCCTTGCTCCAGGTAAAGGGTGAAGG
NFATc4(207–389)	NFAT X-c4-X	Forward: TAAGCGGCCGCCCGCTTTGGCCTGGGCTCC Reverse: TTAGGCGCGCCTTGGACCAAGCGAGTGGG

ligation kit (Roche Applied Science). All NFAT constructs were confirmed by restriction digest and DNA sequencing. There were no significant differences in the expression levels among various NFAT constructs, as confirmed by measuring the fluorescence intensity using identical acquisition settings on an Olympus BX61 microscope equipped with the Fluoview 300 laser scanning confocal imaging system and a 60× oil-immersion objective (NA = 1.4) (supplemental Fig. 2).

Simultaneous EGFP-NFAT and Ca^{2+} Imaging—EGFP-NFATc3- or EGFP-NFATc4-transfected DRG neurons (1–2 DIV) or hippocampal neurons (12–14 DIV) were loaded with the ratiometric Ca^{2+}-indicator dye Fura2-AM (2 μM) for 30 min. Cells were then placed in a chamber for flow-through perfusion and mounted onto an inverted IX-71 microscope (Olympus, Japan). Cells were perfused with a standard extracellular HEPES-buffered Hanks' salt solution composed of (in mM) the following: 140 NaCl, 5 KCl, 1.3 $CaCl_2$, 0.4 $MgSO_4$, 0.5 $MgCl_2$, 0.4 KH_2PO_4, 0.6 $NaHPO_4$, 3 $NaHCO_3$, 10 glucose, 10 HEPES, pH 7.4, with NaOH (310 mosM/kg with sucrose). Fluorescence was sequentially excited at 340 nm (12 nm bandpass), 380 nm (12 nm bandpass), and 475 nm (12 nm bandpass) using a Polychrome IV monochromator (TILL Photonics, Germany) and focused on the cells via a 40× oil-immersion objective (NA = 1.35, Olympus). Fluorescence emission was collected at 530 nm (50 nm bandpass) using an IMAGO CCD camera (640 × 480 pixels; TILL Photonics, Germany). A 2 × 2 binning was used for acquisition (1 pixel ~500 nm). Series of 340, 380, and 475 nm images were acquired every 5 s. $[Ca^{2+}]$ was calculated by converting the fluorescence ratio ($R = F_{340}/F_{380}$) using the following formula: $[Ca^{2+}] = K_d\beta(R - R_{min})/(R_{max} - R)$. R_{min}, R_{max}, and β were calculated by application of 10 μM ionomycin in either Ca^{2+}-free buffer (1 mM EGTA) or in HEPES-buffered Hanks' salt solution (1.3 mM Ca2$^+$). $[Ca^{2+}]_i$ data were analyzed using TILLVision 4.0.12 (TILL Photonics, Germany) software. Cells were stimulated through trains of action potentials induced by field stimulation as described previously (46, 55). NFAT nuclear translocation was quantified by measuring the mean fluorescence intensity of EGFP within the nucleus and cytosol, and data are presented as nuclear/cytosolic ratio. Data were processed using TILLVision 4.0.1.2 (TILL Photonics) software.

Analysis of Depolarization-induced NFAT Translocation in DRG Neurons and PC12 Cells—For microscopy analysis, DRG neurons expressing EGFP-NFAT constructs were stimulated as indicated with 15, 20, or 40 mM K^+. PC12 cells were stimulated with 25 mM K^+ and BayK8644 (1 μM). At different times following stimulation, cells were briefly washed with PBS and fixed in 4% paraformaldehyde for 15 min at room temperature. Cells were then washed extensively with PBS and incubated with a fluorescent DNA-binding probe, DAPI (300 nM; Invitrogen). Coverslips were then mounted onto glass microscope slides using Fluoromount G (Southern Biotechnology Associates, Birmingham, AL). Fluorescence was observed using a 60× oil-immersion objective (NA = 1.4) on an Olympus BX61 microscope equipped with the Fluoview 300 laser scanning confocal imaging system. Data were acquired and analyzed by a blinded experimenter using the Fluoview software (Olympus). Average EGFP fluorescence intensity values for a region of interest in the nucleus, as indicated by DAPI staining, and the cytosol were obtained. Background fluorescence was corrected for using a region of interest devoid of cells.

For biochemical analysis, EGFP-NFATc3- and EGFP-NFATc4-transfected PC12 cells were stimulated with 25 mM KCl and 1 μM BayK8644 for 20 or 180 min, followed by harvesting and fractionation of cytoplasmic and nuclear protein components using the NE-PER nuclear and cytoplasmic extraction kit (Thermo-Pierce), according to the manufacturer's instructions. Normalized quantities of samples were then size-fractionated with 7.5% SDS-PAGE and transferred to nitrocellulose membrane. Blots were incubated with mouse monoclonal anti-GFP (1 μg/ml) and anti-Grp75 (0.5 μg/ml; both Neuromab) and rabbit polyclonal anti-Sp1 transcription factor (1:2000; Millipore) antibodies, followed by washing and incubation with HRP-conjugated secondary antibodies (1:10,000 for goat anti-

mouse IgG and 1:2000 for goat anti-rabbit IgG). Grp75 and Sp1 immunoreactivities were used as cytoplasm- and nucleus-specific markers, respectively. Specific immunoreactive protein bands on membranes were developed with enhanced electrochemiluminescence-plus reagent (PerkinElmer Life Sciences), and the signals were captured on x-ray film (Kodak Biomax; Carestream Health). Densitometric quantification of immunoreactive bands on x-ray films was performed using the intensity measurement function in the ImageJ software (National Institutes of Health). Ratios of nuclear to cytoplasmic GFP-immunoreactive band intensities for each specific treatment time points and transfection types were determined from four independent experiments to perform quantitative and statistical analysis of the data.

Analysis of NFAT Dephosphorylation—PC12 cells were stimulated with 25 mM K^+ and BayK8644 (1 μM) as indicated in high glucose DMEM containing 5% FBS and 10% HS. Some cells were additionally co-treated with FK506 (3 h, 200 nM). Following stimulation, cells were briefly washed in PBS and collected in modified RIPA buffer (1% Triton X-100, 0.1% SDS, 150 mM NaCl, 20 mM Tris-HCl, pH 8.0, protease inhibitor mixture (Pierce), and phosphatase inhibitor mixture (Pierce)). Cells were incubated on ice for 15 min prior to brief sonication. A portion of the lysate from untreated cells expressing HA-NFATc4 and not containing phosphatase inhibitor mixture was incubated with 10 units of alkaline phosphatase (Roche Applied Science) for 3 h at 37 °C. Cell lysate was then diluted with Laemmli reducing sample buffer and incubated at 85 °C for 9 min. Samples were then separated on a 5% SDS-polyacrylamide gel prior to transfer to a nitrocellulose membrane. Nitrocellulose membranes were blocked with 10% milk in Tris-buffered saline (TBS) (20 mM Tris, pH 7.4, 150 mM NaCl) solution for 2 h and then incubated with primary antibody against HA (C12A5 1:10; TC supernatant, Roche Applied Science) or GFP (N86/8, 1:200; Neuromab) in blocking solution containing 0.05% Tween for 2 h. Membranes were then washed and incubated with HRP-conjugated goat anti-mouse secondary antibody (1:5000, Bio-Rad) for 1 h. Membranes were then washed extensively and developed using ECL^+ HRP detection kit (GE Healthcare).

NFAT Reporter Assays—NFAT reporter assays were performed as described previously (46). In brief, DRG or hippocampal neurons were co-transfected with the NFAT-luciferase (NFAT-luc) reporter plasmid (firefly luciferase controlled by three copies of the NFAT-binding motif; pNFAT-TA-luciferase; Clontech), a plasmid encoding a *Renilla reniformis* luciferase controlled by a constitutive HSV-TK promoter (pRL-TK; Promega, Madison, WI), and in some experiments, additionally with NFATc3-shRNA, NFATc4-shRNA, or EGFP-NFATc4 (see "Results" for details). Transfected cell cultures were treated with either vehicle control or with solutions containing increased levels of KCl for 12 h to produce mild depolarization (prepared by mixing 150 mM KCl with complete DMEM, see "Results" for details). The L-type Ca^{2+} channel agonist BayK8644 was added to the depolarization conditions to stabilize $[Ca^{2+}]_i$ at the elevated levels over the duration of stimulation (46). Cells were lysed 12 h after beginning of the stimulation and subsequently analyzed using the Dual-Luciferase protocol (Promega). NFAT-luciferase reporter expression was normalized to that of TK-luc and quantified as the NFAT-luc/TK-luc ratio.

Reagents—Fura-2-AM was obtained from Invitrogen. FK-506 was obtained from Alomone Labs (Israel). Leptomycin B (LMB) was obtained from LC Laboratories (Woburn, MA). All other reagents were obtained from Sigma.

RESULTS

NFATc3, but Not NFATc4, Rapidly Translocates to the Nucleus following Electrical Stimulation of Neurons—We previously reported that NFATc4, in contrast to NFATc1–c3, displayed a distinctly attenuated nuclear translocation in response to 90 mM K^+ stimulation of DRG neurons (46). We decided to test whether NFATc3 and NFATc4 differed in their response to repeated stimulation using trains of action potentials in DRG neurons. We chose to compare the translocation of NFATc4 to that of NFATc3 because NFATc3 is the most abundantly expressed NFAT isoform in DRG neurons, and the translocation of NFATc3 does not qualitatively differ from that of NFATc1 or NFATc2 in DRG neurons (46). We transfected DRG neurons with EGFP-NFATc3 or EGFP-NFATc4 and stimulated cells with 10 trains of action potentials (10 Hz for 10 s, 50 s apart) (Fig. 1, *A* and *B*; supplemental Movies 1 and 2) and simultaneously monitored $[Ca^{2+}]_i$ and EGFP-NFAT subcellular localization. EGFP-NFATc3 rapidly translocated to the nucleus in response to a series of $[Ca^{2+}]_i$ transient elevations induced by repeated trains of action potentials and relocated back to the cytosol following the return of $[Ca^{2+}]_i$ to base line (Fig. 1*A*; supplemental Movie 1). In contrast, we observed no nuclear translocation of EGFP-NFATc4 upon action potential stimulation and resulting $[Ca^{2+}]_i$ transients (Fig. 1*B*; supplemental Movie 2), consistent with our previous observations (46).

To test whether this distinct activation of NFATc3 and NFATc4 is also observed in central neurons, we performed similar experiments in cultured hippocampal neurons (12–14 DIV) transfected with either EGFP-NFATc3 or EGFP-NFATc4. Stimulation using 15 trains of action potentials (10 Hz for 10 s, 50 s apart) (Fig. 1, *C* and *D*) induced rapid nuclear import of EGFP-NFATc3 (Fig. 1*C*). However, as in DRG neurons, action potential stimulation failed to induce nuclear translocation of EGFP-NFATc4 (Fig. 1*D*).

To more thoroughly investigate the apparent distinct regulation of NFATc3 and NFATc4 in neurons, we systematically examined the effects of various levels of depolarization on NFAT translocation during more prolonged stimulation. Bath application of elevated K^+ elicits reproducible elevations in $[Ca^{2+}]_i$ in sensory neurons allowing us to average the subcellular localization of NFAT in response to depolarization of a given intensity and duration (46, 56). We depolarized DRG neurons expressing EGFP-NFATc3 or EGFP-NFATc4 with 15, 20, or 40 mM K^+ and quantified the subcellular localization of NFATc3 and NFATc4 in fixed cells following 20, 60, and 180 min of stimulation. Under basal conditions (5 mM K^+) both EGFP-NFATc3 and EGFP-NFATc4 were excluded from the nucleus, consistent with previous reports (Fig. 2, *A–C*) (45, 46). There was no significant difference between the basal mean nuclear/

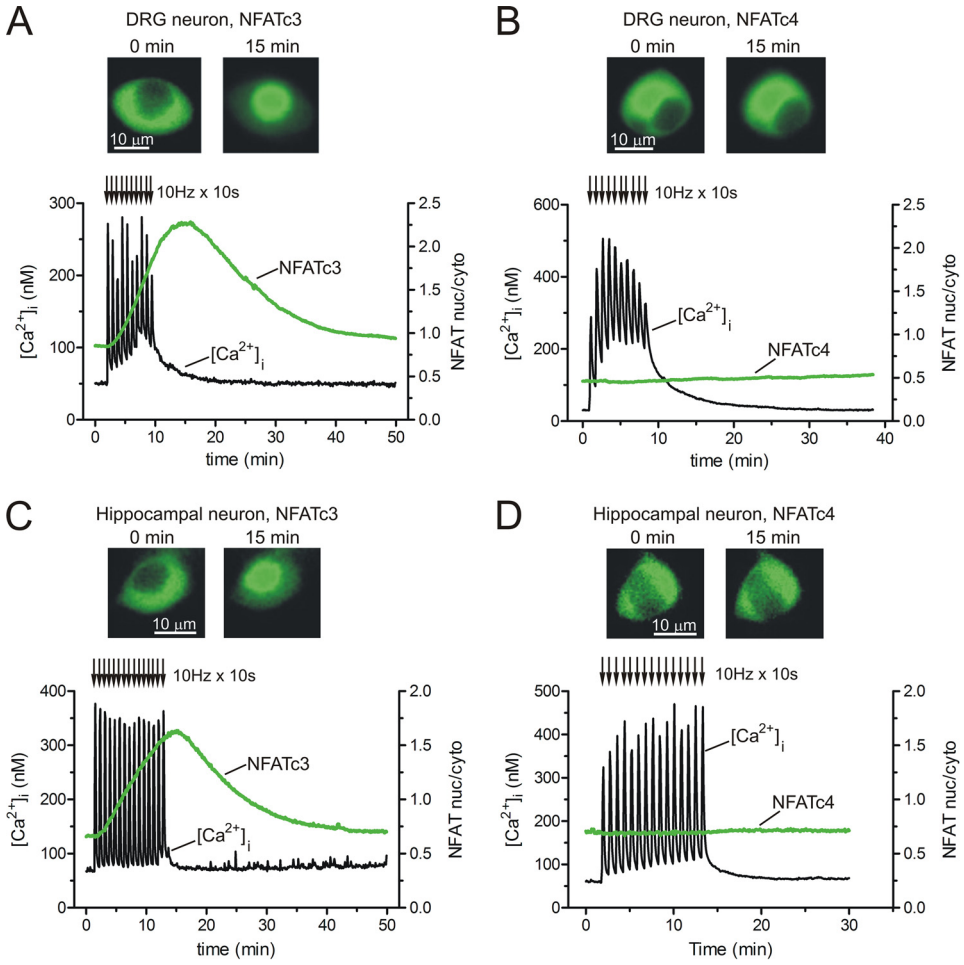

FIGURE 1. **NFATc3, but not NFATc4, translocates to the nucleus upon action potential stimulation of DRG and hippocampal neurons.** *A* and *B,* DRG neurons (1–2 DIV) expressing EGFP-NFATc3 (*A*) or EGFP-NFATc4 (*B*) were stimulated with 10 trains of action potentials (10 Hz for 10 s, 50-s interval, *arrows*). *C* and *D,* hippocampal neurons (12–14 DIV) expressing EGFP-NFATc3 (*C*) or EGFP-NFATc4 (*D*) were stimulated with 15 trains of action potentials (10 Hz × 10 s, 50-s interval, *arrows*). The subcellular localization of EGFP-NFATc3 (*A* and *C*) and EGFP-NFATc4 (*B* and *D*) (*green traces*) was quantified by measuring the mean fluorescence intensity of EGFP within the nucleus or cytosol. Data are presented as mean nuclear/cytosolic fluorescent intensity. $[Ca^{2+}]_i$ (*black trace*) was measured simultaneously with EGFP using the ratiometric indicator dye Fura-2. Images *above* the *traces* show cellular localizations of EGFP-NFATc3 or EGFP-NFATc4 at the indicated time points.

cytosolic ratio of EGFP-NFATc3 and EGFP-NFATc4. Depolarization with 15 mM K^+ for 20 min robustly increased the mean nuclear/cytosolic ratio of EGFP-NFATc3 from 0.52 ± 0.10 (n = 30) under basal conditions to 3.1 ± 0.57 (n = 22) (Fig. 2*A*). Similar results were obtained for EGFP-NFATc3 translocation following a 20-min application of 20 mM K^+ (3.6 ± 0.46, n = 26) (Fig. 2*B*) or 40 mM K^+ (4.3 ± 0.43, n = 24) (Fig. 2*C*). In contrast, EGFP-NFATc4 remained excluded from the nucleus upon 20 min of stimulation with 15 mM K^+ (0.26 ± 0.02, n = 21) (Fig. 2*A*), 20 mM K^+ (0.36 ± 0.03, n = 13) (Fig. 2*B*), or 40 mM K^+ (0.33 ± 0.03, n = 20) (Fig. 2*C*). Prolonged depolarization with 15 mM K^+ for 180 min failed to induce EGFP-NFATc4 nuclear translocation (0.35 ± 0.03, n = 16) (Fig. 2*A*). Increasing the strength of depolarization with 20 mM K^+ (1.0 ± 0.20, n = 24) or 40 mM K^+ (2.0 ± 0.24, n = 30) resulted in a gradual nuclear accumulation of EGFP-NFATc4 over 180 min (Fig. 2, *B* and *C*). However, the nuclear/cytosolic ratio of EGFP-NFATc3 was significantly greater than that of EGFP-NFATc4 throughout the 180-min stimulation with either 20 mM K^+ (3.1 ± 0.65, n = 20) or 40 mM K^+ (6.1 ± 0.67, n = 16) (Fig. 2, *B* and *C*). The amplitudes of the corresponding $[Ca^{2+}]_i$ elevations produced by 15, 20, and 40 mM K^+ in DRG neurons are shown in Fig. 2*D*.

NFAT-mediated Transcription Response to Mild Depolarization Strongly Depends on NFATc3 Isoform in DRG and Hippocampal Neurons—NFATc3 and NFATc4 are the predominant NFAT isoforms in DRG neurons (46). To examine the contribution of endogenous NFATc3 and NFATc4 to depolarization-induced NFAT-mediated transcription responses in neurons, we used an NFAT-luciferase expression reporter assay as described previously (Ref. 46 and also see "Experimental Procedures"). Stimulation of DRG neurons with 20 mM K^+ combined with the L-type Ca^{2+} channel agonist BayK8644 (1 μM) for 12 h produced a nearly 10-fold increase in NFAT-mediated luciferase expression (Fig. 3, *A* and *B*). Knocking down NFATc3 and NFATc4 significantly reduced NFAT-mediated luciferase expression under resting conditions (vehicle treatment) from 0.17 ± 0.01 (NFAT-luc/TK-luc; n = 21) for control cells to 0.08 ± 0.01 and 0.09 ± 0.01 for the cells transfected with NFATc3-shRNA (n = 7; $p < 0.001$) or NFATc4-shRNA (n = 7; $p < 0.001$), respectively (Fig. 3*A*). More importantly, knocking

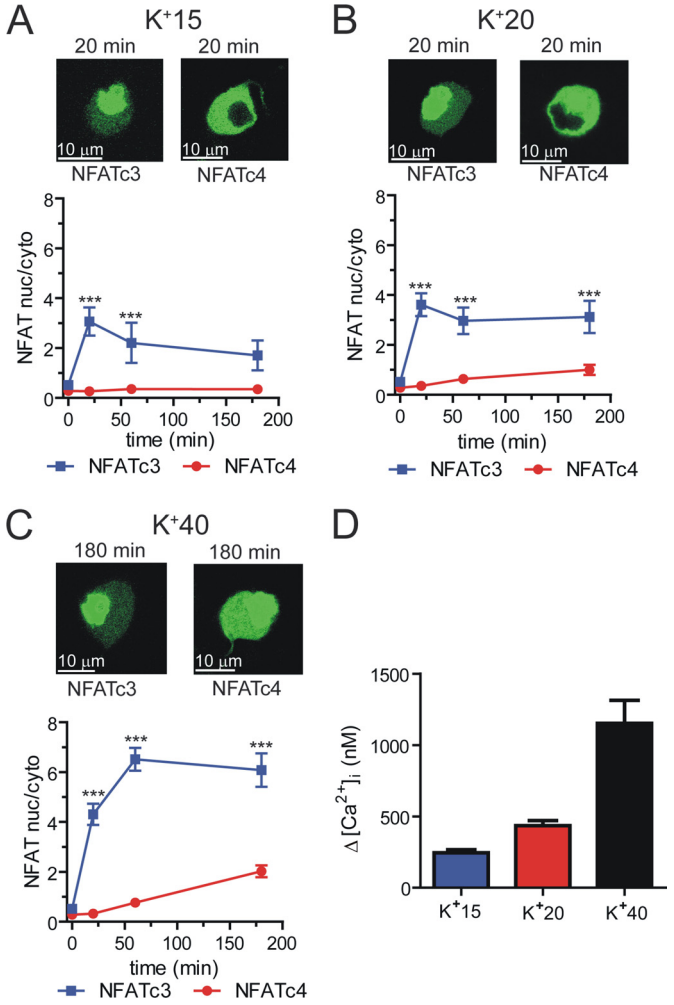

FIGURE 2. **Differential nuclear translocation of NFATc3 and NFATc4 in response to depolarization.** *A–C,* DRG neurons (1 DIV) overexpressing EGFP-NFATc3 or EGFP-NFATc4 were stimulated with 15 mM (*A*), 20 mM (*B*), or 40 mM (*C*) K^+ for 20, 60, or 180 min. Data points represent mean nuclear/cytosolic (*nuc/cyto*) fluorescence intensity ± S.E. (n = 15–40 cells). Images show typical distributions of EGFP-NFATc3 and EGFP-NFATc4 for specified treatments and time points. ***, $p < 0.001$, one-way ANOVA followed by Bonferroni post hoc test between isoforms for each time point. *D,* amplitudes of $[Ca^{2+}]_i$ elevations produced by K^+15, K^+20, and K^+40 depolarization in DRG neurons ($\Delta[Ca^{2+}]_i$). $[Ca^{2+}]_i$ was measured in DRG neurons under conditions similar to that of DRG cell culture. Cell culture medium was supplemented with 20 mM HEPES, pH 7.4, and perfused at 37 °C. $[Ca^{2+}]_i$ measurements were taken 20 min after depolarization with K^+15, K^+20, or K^+40 (n = 15–26 cells).

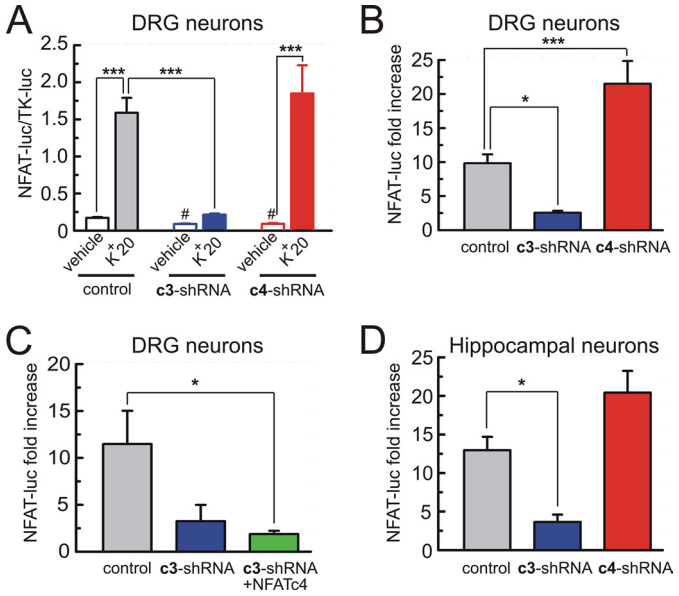

FIGURE 3. **Activation of NFAT-mediated transcription by mild depolarization in neurons strongly depends on NFATc3.** *A,* Dual-Luciferase assay was performed in DRG neurons stimulated with either a vehicle or with 20 mM KCl and 1 μM BayK8644 (K^+20) for 12 h. Control cells were transfected with NFAT-luciferase (firefly; *NFAT-luc*) and TK-luciferase (*Renilla*, *TK-luc*) only, whereas two other groups were additionally transfected with an shRNA construct targeting either NFATc3 (*c3-shRNA*, *blue*) or NFATc4 (*c4-shRNA*, *red*). NFAT transcription activation was quantified as the NFAT-luc/TK-luc luminescence intensity ratio. ***, $p < 0.001$, one-way ANOVA with Bonferroni's post test; #, $p < 0.001$, one-way ANOVA with Bonferroni's post test relative to vehicle control (n = 7–21 experiments for various treatment groups). *B,* data from experiments in *A* were re-analyzed by normalizing NFAT-luciferase activity in K^+20 + BayK8644-stimulated cells relative to unstimulated cells (vehicle). *, $p < 0.05$; ***, $p < 0.001$, one-way ANOVA with Bonferroni's post hoc test (n = 7–21 independent experiments). *C,* NFAT-luciferase activity in DRG neurons treated with 40 mM KCl for 12 h were normalized to that in unstimulated cells. Three groups of neurons were compared as follows: transfected with NFAT-luc/TK-luc only (*control*); NFAT-luc/TK-luc co-transfected with NFATc3 shRNA (*c3-shRNA*, *blue*); and NFAT-luc/TK-luc co-transfected with NFATc3 shRNA and EGFP-NFATc4 (*c3-shRNA* + *NFATc4*, *green*). *, $p < 0.05$, one-way ANOVA with Bonferroni's post hoc test (n = 3–6 experiments). *D,* NFAT-luciferase activity in hippocampal neurons treated with 25 mM KCl and 1 μM BayK8644 for 12 h was normalized to that in unstimulated neurons. Three groups of hippocampal neurons were examined as follows: transfected with NFAT-luc/TK-luc only (*control*, *gray*) and those co-transfected with shRNA plasmid targeting either NFATc3 (*c3-shRNA*, *blue*) or NFATc4 (*c4-shRNA*, *red*). *, $p < 0.05$, one-way ANOVA with Bonferroni's post hoc test (n = 3–5 experiments).

down NFATc3, but not NFATc4, significantly diminished the depolarization-induced increase in NFAT-mediated luciferase expression in DRG neurons. The NFATc3-shRNA effect could not be rescued by overexpressing NFATc4 in these cells (Fig. 3*C*). Similar to effects in DRG neurons, knocking down NFATc3, but not NFATc4, in hippocampal neurons significantly reduced depolarization-induced expression of NFAT-luciferase reporter (Fig. 3*D*). Overall, these results suggest that NFATc3 is a major contributor to NFAT-mediated transcription response induced by mild depolarization in DRG and hippocampal neurons. In contrast, the contribution of NFATc4 is minimal under these conditions, which is consistent with the blunted activation of this isoform in response to mild depolarization (Fig. 2).

NFAT Homology Region Determines the Rate and Amplitude of NFATc3 and NFATc4 Translocation—NFAT activation is dependent on CaN-mediated dephosphorylation of multiple serine residues flanking an NLS within the NHR (57, 58). Therefore, we hypothesized that the NHR was responsible for the difference in depolarization-induced translocation observed for NFATc3 and NFATc4. To test this hypothesis, we generated two NFAT chimeras as follows: one in which amino acids 1–403 of NFATc3 were replaced with amino acids 1–388 of NFATc4 (NFATc3-NHRc4), and a second in which amino acids 1–388 of NFATc4 were replaced with amino acids 1–403 of NFATc3 (NFATc4-NHRc3) (Fig. 4*A*). We then transfected DRG neurons with these chimeras and monitored their subcellular localization in response to depolarization.

Both EGFP-NFATc4-NHRc3 (0.30 ± 0.02, n = 26) and EGFP-NFATc3-NHRc4 (0.28 ± 0.03, n = 17) were excluded from the nucleus under basal conditions (Fig. 4*B*). Depolarization with 20 mM K^+ resulted in a strong increase in the mean

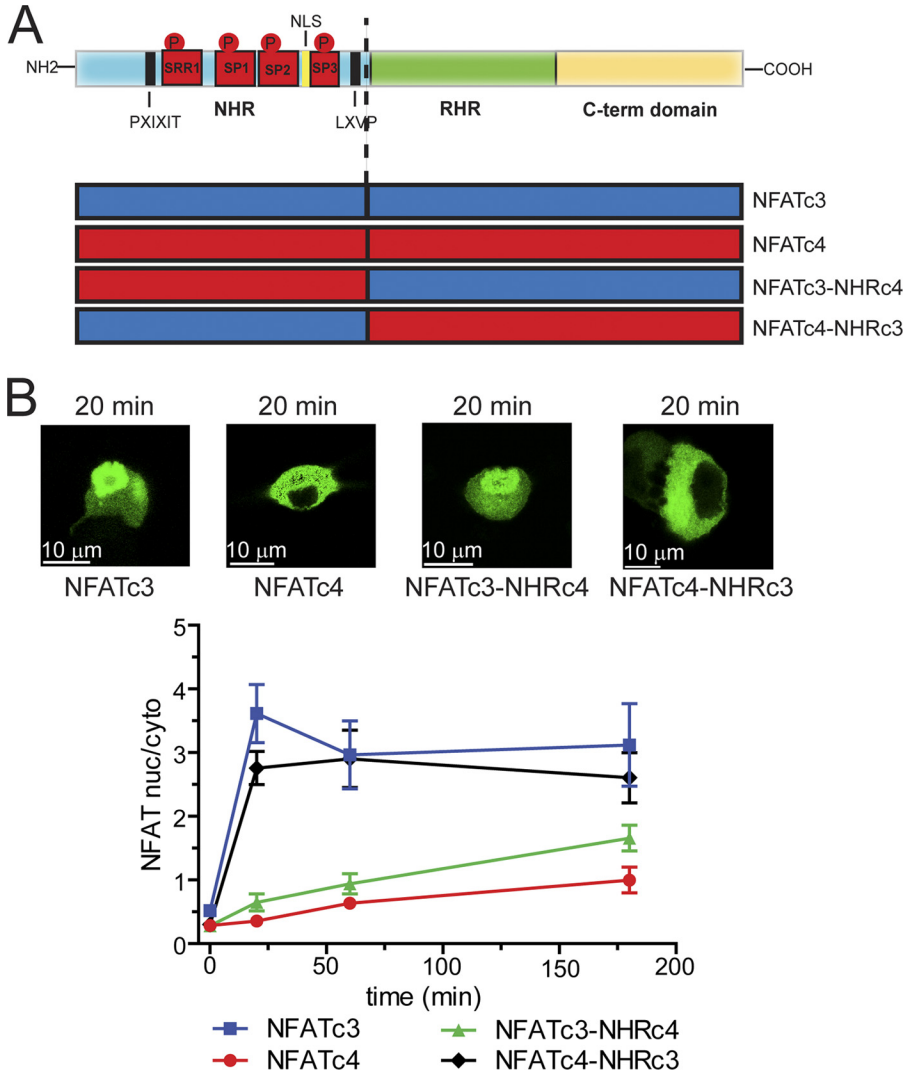

FIGURE 4. **NFAT homology region determines the rate and amplitude of NFATc3 and NFATc4 nuclear translocation.** *A,* schematic of NFAT homology region (*NHR*) chimeras. NFATc3-NHRc4 consists of the NFATc3 protein in which the NFATc3 NHR-containing region (1–403) has been exchanged for that of NFATc4 NHR (1–388). NFATc4-NHRc3 consists of the NFATc4 protein in which the NFATc4 NHR-containing region (1–388) has been exchanged for that of NFATc3(1–403). *B,* DRG neurons (1 DIV) transfected with EGFP-NFATc3, EGFP-NFATc4, EGFP-NFATc3-NHRc4, or EGFP-NFATc4-NHRc3 were stimulated with 20 mM K^+ for 20, 60, or 180 min. Representative images show cellular distribution of specific NFAT constructs after 20 min of stimulation with 20 mM K^+. Data points represent mean nuclear/cytosolic fluorescence intensity ± S.E. (n = 10–40 cells).

nuclear/cytosolic ratio of EGFP-NFATc4-NHRc3 at 20 min (2.7 ± 0.26, n = 29), similar to the response of EGFP-NFATc3 to depolarization (Fig. 4*B*). EGFP-NFATc4-NHRc3 remained predominantly localized in the nucleus through 180 min of depolarization (2.6 ± 0.39, n = 22) (Fig. 4*B*). In contrast, EGFP-NFATc3-NHRc4 remained excluded from the nucleus following 20 min of depolarization (0.65 ± 0.13, n = 23) and gradually accumulated in the nucleus through 180 min of depolarization (1.7 ± 0.20, n = 41), similar to EGFP-NFATc4 (Fig. 4*B*). These data demonstrate that the NHR is responsible for the differential sensitivity of NFATc3 and NFATc4 to depolarization.

Differential Dephosphorylation of NFATc3 and NFATc4 following Depolarization—CaN-mediated dephosphorylation of the NFAT NHR is critical for translocation of NFAT from the cytosol to the nucleus (13, 59). Because NFATc4 translocates to the nucleus at a strikingly slower rate than NFATc3, we asked whether NFATc3 and NFATc4 were differentially dephosphorylated upon depolarization. We tested our hypothesis by using the neuron-like PC12 cell line to obtain enough material for biochemical analysis. Because NFAT proteins are heavily phosphorylated (57), dephosphorylation results in a readily apparent increase in the electrophoretic mobility of NFAT.

We first tested whether EGFP-NFATc3 and EGFP-NFATc4 were differentially activated by depolarization in PC12 cells similar to our observations in DRG and hippocampal neurons. PC12 cells transfected with EGFP-NFATc3 or EGFP-NFATc4 were stimulated with 25 mM K^+ and BayK8644 (1 μM) to reduce inactivation of voltage-gated Ca^{2+} influx. Both EGFP-NFATc3 (0.28 ± 0.01, n = 31) and EGFP-NFATc4 (0.28 ± 0.02, n = 30) were excluded from the nucleus under basal conditions (Fig. 5*A*). Stimulation for 20 min resulted in a strong increase in the nuclear localization of EGFP-NFATc3 (4.4 ± 0.33, n = 32) but not EGFP-NFATc4 (0.29 ± 0.01, n = 30) (Fig. 5*A*). EGFP-NFATc4 remained excluded from the nucleus upon stimulation for 180 min (0.29 ± 0.02, n = 31) (Fig. 5*A*). To further confirm the observed difference in nuclear translocation, we

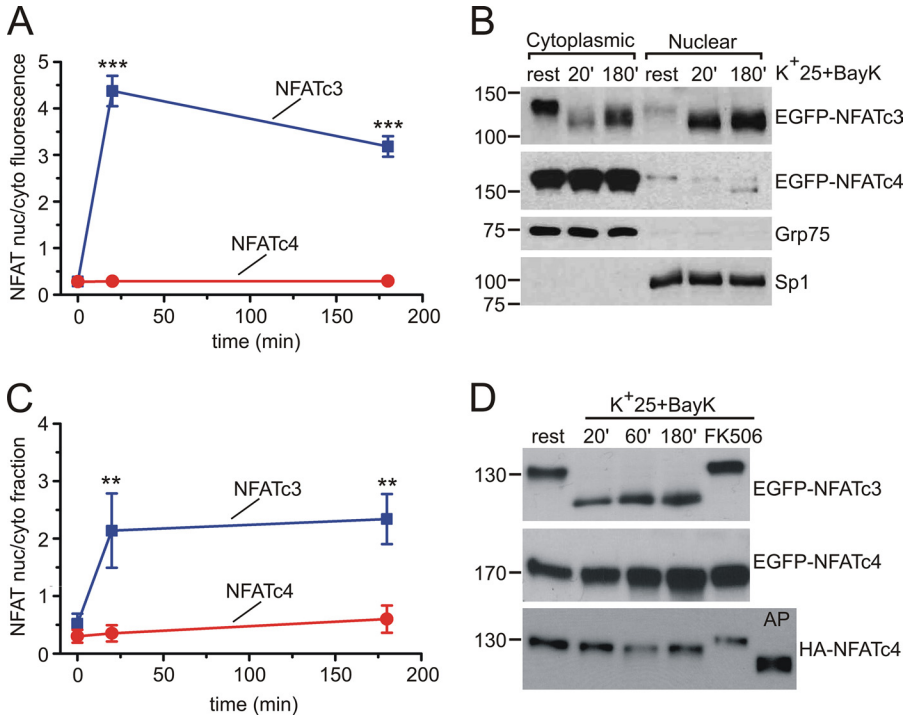

FIGURE 5. **Rapid dephosphorylation of NFATc3, but not NFATc4, in response to depolarization.** *A,* PC12 cells overexpressing EGFP-NFATc3 or EGFP-NFATc4 were stimulated with 25 mM K^+ and BayK8644 (1 μM) for 20 or 180 min. Data points represent mean nuclear/cytosolic (*nuc/cyto*) fluorescence intensity ± S.E. ($n = 30–32$ cells) and were compared by ANOVA followed by Bonferroni post hoc test between isoforms for each time point. ***, $p < 0.001$. *B,* PC12 cells transfected with EGFP-NFATc3 or EGFP-NFATc4 either remained untreated (*rest*) or were stimulated using 25 mM K^+ and BayK8644 (1 μM) for 20 or 180 min. Following stimulation, nuclear and cytoplasmic fractions were separated, and immunoblotting against EGFP was performed. Fractionation was validated by immunoblotting against the cytosolic protein Grp75 and the nuclear protein Sp1. *C,* densitometry was used to determine the EGFP-NFAT content of the cytoplasmic and nuclear fractions for the experiments described in *B,* and the nuclear/cytoplasmic ratio for NFATc3 (*blue*) and NFATc4 (*red*) was compared at various times of stimulation with 25 mM K^+ and 1 μM BayK8644 ($t = 0$ min corresponds to the resting condition). **, $p < 0.01$, one-way ANOVA with Bonferroni post hoc test ($n = 4$ independent experiments for each NFAT isoform; mean ± S.E.). *D,* electrophoretic mobility of EGFP-NFATc3 is strongly increased upon depolarization for 20, 60, or 180 min with 25 mM K^+ and BayK8644 (1 μM), indicative of dephosphorylation. Co-application of the CaN inhibitor FK506 (200 nM) for 180 min blocked the depolarization-dependent dephosphorylation. In contrast, K^+25 + BayK8644 (1 μM) stimulation failed to noticeably increase the electrophoretic mobility of EGFP-NFATc4 or HA-NFATc4. Treatment of cell lysate with alkaline phosphatase (*AP*) increased the mobility of HA-NFATc4.

biochemically analyzed the subcellular localization of EGFP-NFATc3 and EGFP-NFATc4 by nuclear/cytoplasmic fractionation. We found that depolarization induced a rapid reduction of NFATc3 in cytoplasmic fraction, whereas the amount of NFATc3 in nuclear fraction markedly increased (Fig. 5, *B* and *C*). In contrast, depolarization had only a minor effect on the distribution of NFATc4 between cytoplasmic and nuclear fractions (Fig. 5, *B* and *C*).

After confirming that EGFP-NFATc3 and EGFP-NFATc4 were differentially activated by depolarization in PC12 cells, we tested whether they were also differentially dephosphorylated following depolarization. The electrophoretic mobility of EGFP-NFATc3 was markedly increased following 20 min of stimulation, indicative of dephosphorylation (Fig. 5*D*). The increase in mobility was blocked by co-treatment with the CaN inhibitor FK506 (200 nM) (Fig. 5*D*). In contrast, there was no apparent increase in the mobility of EGFP-NFATc4 after stimulation (Fig. 5*D*). We speculated that perhaps the shift in electrophoretic mobility for NFATc4 was masked by the large molecular weight of the EGFP-NFATc4 fusion protein. We therefore repeated the assay with the smaller HA-NFATc4 and again did not detect a significant change in the electrophoretic mobility upon stimulation (Fig. 5*D*). Co-treatment with FK506 (200 nM) resulted in a slight but consistent decrease in HA-NFATc4 mobility indicative of a possible basal level of CaN-dependent dephosphorylation of NFATc4 (Fig. 5*D*) (37). To test whether HA-NFATc4 was already dephosphorylated under basal conditions, we incubated untreated cell lysate with alkaline phosphatase. The electrophoretic mobility of alkaline phosphatase-treated HA-NFATc4 was increased compared with that of control, indicating that NFATc4 was not fully dephosphorylated under basal conditions in PC12 cells (Fig. 5*D*). Thus, the rapid and robust dephosphorylation of EGFP-NFATc3 and the incomplete dephosphorylation of EGFP-NFATc4 and HA-NFATc4 in PC12 cells are consistent with the observed difference in NFATc3 and NFATc4 translocation in hippocampal and DRG neurons.

NFATc3 CaN-binding Motifs Are Insufficient to Facilitate Nuclear Translocation of NFATc4—Because NFATc3 and NFATc4 are differentially dephosphorylated upon depolarization-dependent $[Ca^{2+}]_i$ elevation, we asked whether differences in the CaN-binding motifs between NFATc3 and NFATc4 were important for their distinct regulation. NFATc3 and NFATc4 contain two CaN-binding motifs, an activity-dependent L*X*VP site in the C-terminal region of the NHR and a P*X*I*X*IT motif in the N-terminal region, which is critical for NFAT dephosphorylation (30–32, 61, 62). The NFATc4 P*X*I*X*IT motif is unique among NFAT isoforms in that the sec-

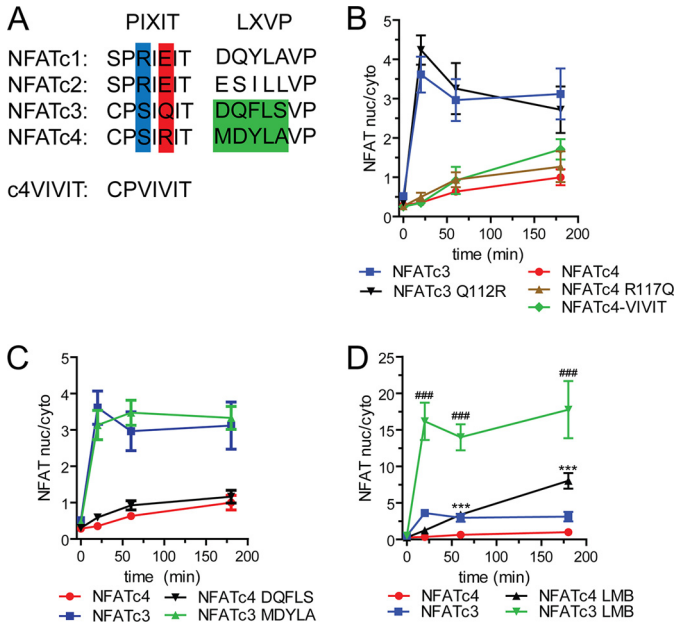

FIGURE 6. **Differential translocation of NFATc3 and NFATc4 is not mediated by differences in the P*XIXIT* or L*XVP* motifs.** *A*, alignment of the P*XIXIT* and L*XVP* motifs of NFATc1-NFATc4 and the high affinity PVIVIT motif. *B*, DRG neurons (1 DIV) transfected with EGFP-NFATc3, EGFP-NFATc4, EGFP-NFATc3-Q112R, EGFP-NFATc4-VIVIT, or EGFP-NFATc4-R117Q were stimulated for 20, 60, or 180 min with 20 mM K^+. Data points represent mean nuclear/cytosolic (*nuc/cyto*) fluorescence intensity ± S.E. (n = 9–40 cells). Data were analyzed by ANOVA of NFAT isoforms for each time point followed by Bonferroni post hoc test between mutant and wild-type NFATc4 and mutant and wild-type NFATc3. *C*, DRG neurons (1 DIV) transfected with EGFP-NFATc3, EGFP-NFATc4, EGFP-NFAT-MDYLA, or EGFP-NFATc4-DQFLS were stimulated for 20, 60, or 180 min with 20 mM K^+. Data were analyzed by ANOVA of NFAT isoforms for each time point followed by Bonferroni post hoc test between mutant and wild-type NFATc4 and mutant and wild-type NFATc3. *D*, DRG neurons (1 DIV) transfected with EGFP-NFATc3 or EGFP-NFATc4 were stimulated for 20, 60, or 180 min with 20 mM K^+ and LMB (100 nM). Data points represent mean nuclear cytosolic fluorescence intensity ± S.E. (n = 13–40 cells). ###, $p < 0.001$, and ***, $p < 0.001$, one-way ANOVA followed by Bonferroni post hoc test between LMB-treated and untreated cells for each time point (### for NFATc3 and *** for NFATc4).

ond variable residue, Arg-117, is positively charged, whereas the other NFAT isoforms contain negatively charged or neutral amino acids in the second variable position (Fig. 6*A*). We hypothesized that the difference in P*XIXIT* charge could affect CaN binding and thus affect the ability of CaN to dephosphorylate NFATc4 *versus* NFATc3.

We generated EGFP-NFATc4-R117Q to create an NFATc4 construct containing the P*XIXIT* motif of NFATc3. Under basal conditions, EGFP-NFATc4-R117Q was excluded from the nucleus (0.27 ± 0.04, n = 11) (Fig. 6*B*). The nuclear localization of EGFP-NFATc4-R117Q following 20 min of depolarization with 20 mM K^+ (0.50 ± 0.11, n = 17) was not significantly different from that of EGFP-NFATc4 (Fig. 6*B*). Prolonged depolarization for 180 min resulted in a gradual nuclear accumulation of EGFP-NFATc4-R117Q (1.3 ± 0.40, n = 17), which did not differ significantly from translocation of EGFP-NFATc4 (Fig. 6*B*). Therefore, substitution of the P*XIXIT* motif of NFATc3 for that of NFATc4 did not affect the rate or amplitude of NFATc4 nuclear translocation. Moreover, in reverse experiments, a Q112R mutation in the P*XIXIT* region of NFATc3 (EGFP-NFATc3-Q112R) did not significantly affect its nuclear translocation in response to depolarization (Fig. 6*B*).

Substitution of valine for the variable residues of the P*XIXIT* motif increases the affinity of NFAT for CaN and increases the ability of CaN to dephosphorylate NFAT (25, 63, 64). We replaced the variable residues of the NFATc4 P*XIXIT* motif with valine residues (EGFP-NFATc4-VIVIT) and analyzed the subcellular localization of EGFP-NFATc4-VIVIT in DRG neurons upon depolarization. Under basal conditions, EGFP-NFATc4-VIVIT was excluded from the nucleus (Fig. 6*B*). Depolarization with 20 mM K^+ for 20 min did not result in a significant nuclear accumulation of EGFP-NFATc4-VIVIT (0.35 ± 0.03, n = 9), and 180 min of depolarization resulted in a gradual nuclear accumulation of EGFP-NFATc4-VIVIT, which did not differ significantly from EGFP-NFATc4 (1.7 ± 0.26, n = 32) (Fig. 6*B*). Taken together, these data suggest that the distinct response of NFATc3 and NFATc4 is not attributable to differences in the affinity of CaN for the P*XIXIT* motif.

A previous study suggested that the L*XVP* motifs in NFATc3 and NFATc4 have equivalent affinities for CaN *in vitro* (30). However, it is possible that in the cellular context differences in the L*XVP* motif between NFATc3 and NFATc4 could contribute to differential CaN-mediated dephosphorylation. Both NFATc1 and NFATc3 contain Asp and Gln residues in the −3 and −2 positions upstream of the L*XVP* motif (Fig. 6*A*). In contrast, NFATc4 contains Met and Asp in these positions (Fig. 6*A*). To test whether differences in the L*XVP* motif contributed to differential NFATc3 and NFATc4 activation, we generated an NFATc4 mutant in which the L*XVP* motif of NFATc4 was replaced with that of NFATc3 (EGFP-NFATc4-DQFLS).

Under basal conditions, EGFP-NFATc4-DQFLS was predominantly localized in the cytosol (0.31 ± 0.02, n = 9) (Fig. 6*C*). The nuclear localization of EGFP-NFATc4-DQFLS upon depolarization with 20 mM K^+ for 20 min (0.59 ± 0.08, n = 10), 60 min (0.92 ± 0.13, n = 21), and 180 min (1.2 ± 0.18, n = 18) was not significantly different from that of EGFP-NFATc4 (Fig. 6*C*). To test whether the L*XVP* motif of NFATc4 was sufficient to inhibit nuclear translocation, we generated an NFATc3 mutant in which the L*XVP* motif of NFATc3 was replaced with that of NFATc4 (EGFP-NFATc3-MDYLA). The nuclear localization of EGFP-NFATc3-MDYLA was not significantly different from that of EGFP-NFATc3 under basal (0.46 ± 0.07, n = 12) conditions or upon 20 mM K^+ stimulation for 20 min (3.1 ± 0.40, n = 12), 60 min (3.5 ± 0.35, n = 15), and 180 min (3.3 ± 0.31, n = 16) (Fig. 6*C*). These data support the conclusion that the differential nuclear translocation of NFATc3 and NFATc4 is not attributable to isoform-dependent differences in CaN binding.

Differential Rate of Nuclear Import for NFATc3 and NFATc4 Contributes to Distinct Activation Kinetics—The nuclear and cytosolic distribution of NFAT is determined by the relative rate of NFAT nuclear import and export. Therefore, the unresponsiveness of NFATc4 to depolarization could arise from a slow nuclear import, fast nuclear export, or combination of the two. To test whether a robust export alone accounted for the slow NFATc4 nuclear translocation, we depolarized cells in the presence of LMB, which blocks NFAT nuclear export via irreversible inhibition of Crm1 (65). LMB (100 nM) application significantly increased the depolarization-induced translocation of EGFP-NFATc4 at 60 min (3.4 ± 0.26, n = 22) and 180

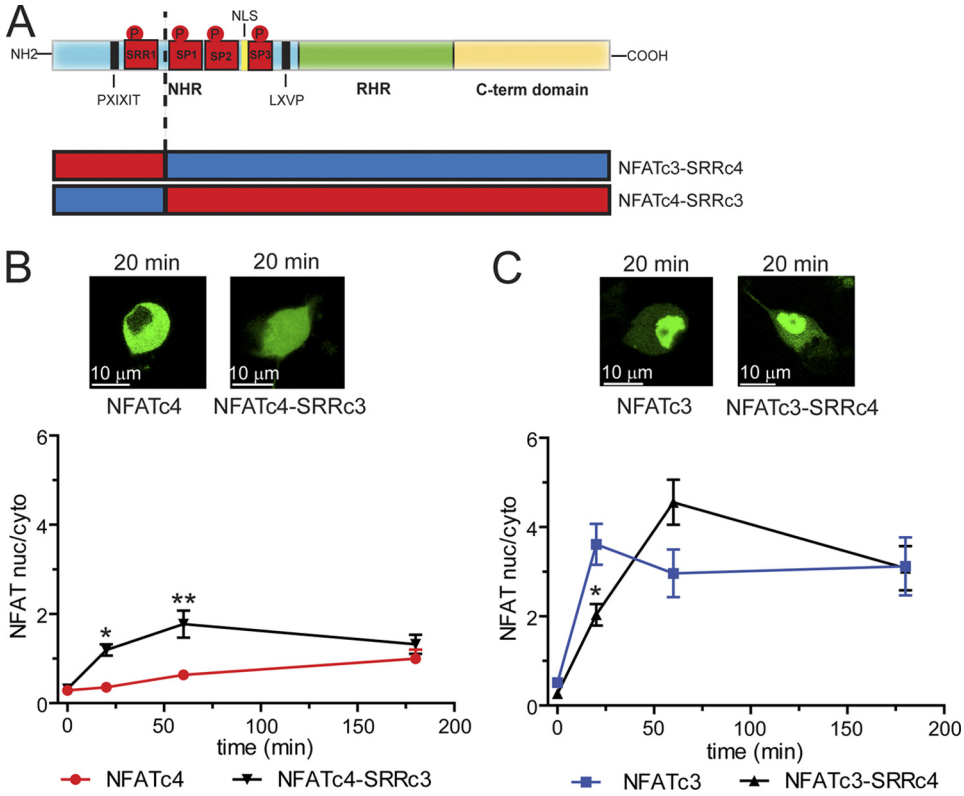

FIGURE 7. **N-terminal half of the NHR regulates early NFAT nuclear translocation.** *A*, schematic of NFAT chimera construction. *B* and *C*, DRG neurons (1 DIV) expressing EGFP-NFATc4-SRRc3 (*B*) or EGFP-NFATc3-SRRc4 (*C*) were stimulated for 20, 60, or 180 min with 20 mM K^+. The corresponding time courses of NFATc4 (*B*) and NFATc3 (*C*) were re-plotted from Fig. 2*B* for comparison. Data points represent mean nuclear/cytosolic (*nuc/cyto*) fluorescence intensity ± S.E. (n = 13–46 cells) *, $p < 0.05$; **, $p < 0.01$, one-way ANOVA followed by Bonferroni post hoc test between isoforms for each time point.

min (8.0 ± 0.92, n = 29) (Fig. 6*D*). However, LMB treatment only slightly increased the nuclear translocation of EGFP-NFATc4 following 20 min of depolarization (1.2 ± 0.21, n = 17) (Fig. 6*D*), and the nuclear localization of EGFP-NFATc4 remained lower than that of NFATc3, even in the presence of LMB. In contrast, LMB treatment dramatically increased the level of EGFP-NFATc3 nuclear translocation at 20 min (16.2 ± 2.6, n = 11) (Fig. 6*D*). There was no further increase in EGFP-NFATc3 nuclear translocation following 60 min (14.0 ± 1.8, n = 10) or 180 min (17.8 ± 3.9, n = 10) of stimulation, suggesting that EGFP-NFATc3 nuclear localization was maximal by at least 20 min, in contrast to the slow and steady increase in EGFP-NFATc4 nuclear localization through 180 min (Fig. 6*D*). These results suggest that the overall diminished depolarization-induced activation of NFATc4 in neurons is attributable in part to a relatively slow nuclear import of this isoform.

Differential Contribution of the N- and C-terminal Halves of the NFAT Homology Region to NFAT Activation—Our data indicated that NFATc3 and NFATc4 were differentially dephosphorylated in response to depolarization-induced $[Ca^{2+}]_i$ elevation (Fig. 5*D*). NFAT proteins contain two major phosphoserine-containing regions as follows: SRR1 localized in the N-terminal half of the NHR and SP1–SP3 localized in the C-terminal half of the NHR. We replaced amino acids 1–206 of NFATc4, containing SRR1, with the homologous region of NFATc3 (amino acids 1–200; EGFP-NFATc4-SRRc3) (Fig. 7*A*) and analyzed the subcellular localization of EGFP-NFATc4-SRRc3 in response to depolarization with 20 mM K^+. Under basal conditions, EGFP-NFATc4-SRRc3 was localized to the cytosol (0.32 ± 0.02, n = 20) (Fig. 7*B*). Following a 20-min (1.2 ± 0.13, n = 46) or 60-min (1.8 ± 0.30, n = 32) depolarization, the nuclear localization of EGFP-NFATc4-SRRc3 was significantly greater than that of EGFP-NFATc4 (Fig. 7*B*). However, after a 180-min stimulation, there was no significant difference between the nuclear localization of EGFP-NFATc4-SRRc3 (1.3 ± 0.21, n = 36) and EGFP-NFATc4 (Fig. 7*B*).

Because replacement of the N-terminal half of the NFATc4 NHR with that of NFATc3 increased depolarization-dependent NFATc4 nuclear localization, we asked whether substitution of the N-terminal half of the NFATc4 NHR for that of NFATc3 would inhibit NFATc3 nuclear translocation. We generated a construct in which amino acids 1–200 of NFATc3 were replaced with the homologous region of NFATc4 (amino acids 1–206; EGFP-NFATc3-SRRc4) (Fig. 7*A*) and assessed the subcellular localization of EGFP-NFATc3-SRRc4 in response to depolarization. EGFP-NFATc3-SRRc4 was localized to the cytosol under basal conditions (0.26 ± 0.02, n = 19) and did not differ significantly from EGFP-NFATc3 (Fig. 7*C*). Following a 20-min depolarization with 20 mM K^+, the nuclear/cytosolic ratio of EGFP-NFATc3-SRRc4 (2.0 ± 0.24, n = 45) was significantly less than that of EGFP-NFATc3 (Fig. 7*C*). However, the nuclear localization of EGFP-NFATc3-SRRc4 did not differ significantly from that of EGFP-NFATc3 following 60 min (4.6 ± 0.50, n = 28) or 180 min (3.1 ± 0.50, n = 34) of stimulation (Fig. 7*C*). Taken together, these data suggest that the N-terminal portion of the NHR, which contains SRR1, affects the initial

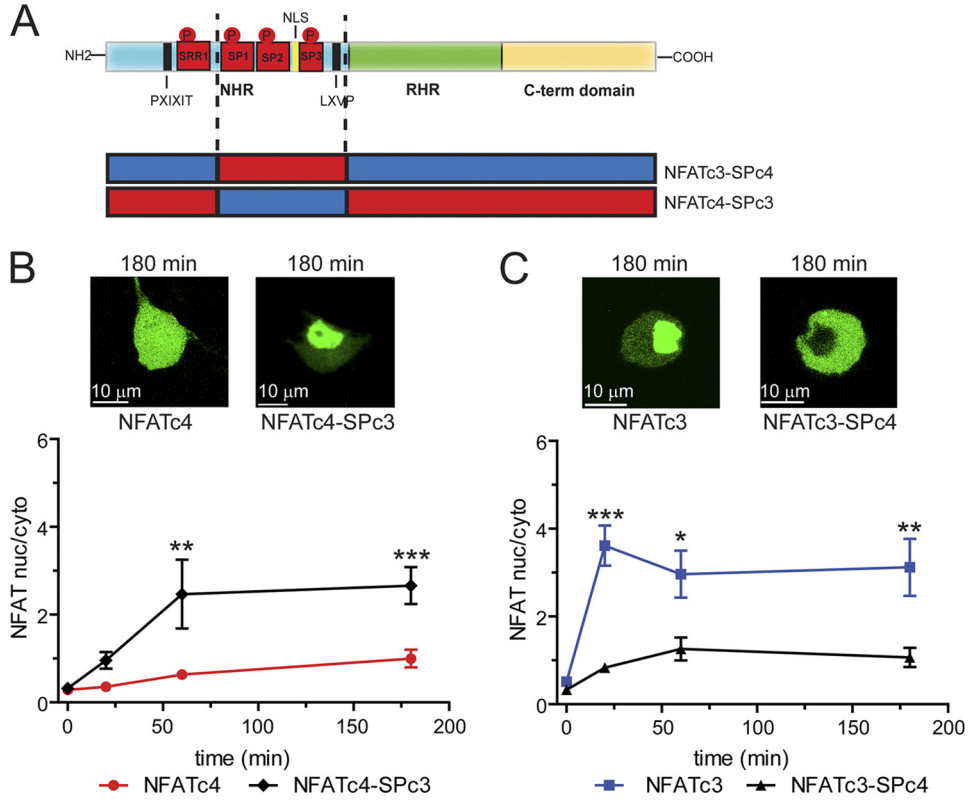

FIGURE 8. **C-terminal half of the NHR determines the rate and magnitude of NFAT nuclear translocation.** *A,* schematic of NFAT chimera construction. *B* and *C,* DRG neurons (1 DIV) expressing EGFP-NFATc4-SPc3 (*B*) or EGFP-NFATc3-SPc4 (*C*) were stimulated with 20 mM K^+ for 20, 60, or 180 min. The translocation time course of the corresponding wild-type NFAT isoforms was re-plotted from Fig. 2*B* to enable comparison with the described NFAT chimeras. Data points represent mean nuclear/cytosolic (*nuc/cyto*) fluorescence intensity ± S.E. (n = 13–36 cells). *, $p < 0.05$; **, $p < 0.01$; ***, $p < 0.001$, one-way ANOVA followed by Bonferroni post hoc test between isoforms for each time point. Images *above* the plots show typical cellular distribution of the indicated NFAT constructs after 180 min following 20 mM K^+ stimulation.

nuclear translocation of NFAT but not the amplitude of NFAT nuclear localization upon prolonged depolarization.

We next examined whether the C-terminal portion of the NHR contributed to the slow kinetics of NFATc4 translocation. We generated an NFAT chimera where amino acids 207–388 of NFATc4, which contains the SP motifs, were replaced with the homologous region of NFATc3 (amino acids 201–403; EGFP-NFATc4-SPc3) (Fig. 8*A*). EGFP-NFATc4-SPc3 was excluded from the nucleus under basal conditions (0.32 ± 0.02, n = 15) (Fig. 8*B*). There was a slight increase in the nuclear localization of EGFP-NFATc4-SPc3 following 20 min of stimulation (0.96 ± 0.19, n = 25). However, there was a significant increase in the nuclear localization of EGFP-NFATc4-SPc3 following 60 min (2.5 ± 0.78, n = 15) or 180 min (2.7 ± 0.42, n = 36) of depolarization with 20 mM K^+ (Fig. 8*B*). Therefore, the C-terminal half of NFATc3 was able to increase the nuclear localization of NFATc4 upon prolonged depolarization.

To test whether the C-terminal half of the NFATc4 NHR could inhibit NFATc3 translocation, we generated a chimera in which amino acids 201–403 of NFATc3 were replaced with the homologous region of NFATc4 (amino acids 207–388; EGFP-NFATc3-SPc4) (Fig. 8*A*). The depolarization-induced nuclear translocation of EGFP-NFATc3-SPc4 was significantly reduced as compared with EGFP-NFATc3 at 20 min (0.83 ± 0.11, n = 24), 60 min (1.3 ± 0.26, n = 16), and 180 min (1.1 ± 0.22, n = 34) (Fig. 8*C*). Taken together, these data demonstrate that the C-terminal half of the NFATc4 NHR was critical for repressing NFATc4 activation in neurons.

Knockdown of GSK3β Strongly Facilitates Nuclear Translocation of NFATc4—Given that the C-terminal half of the NHR, which contains the SP1–SP3 phosphoserine motifs, appeared to be critical for the repression of NFATc4, we asked whether kinases that phosphorylate the SP motifs repressed NFATc4 nuclear localization. GSK3β phosphorylates the SP motifs of NFAT, which is thought to oppose nuclear localization of NFAT (5, 38). We hypothesized that GSK3β activity could oppose CaN-mediated dephosphorylation of NFATc4 and thus maintain NFATc4 in a phosphorylated and nuclear excluded state in neurons. To test this hypothesis, we co-transfected DRG neurons with EGFP-NFATc4 and an shRNA construct targeting GSK3β (supplemental Fig. 1). Knockdown of GSK3β had no effect on the basal localization of EGFP-NFATc4 (0.41 ± 0.07, n = 9) but increased the nuclear localization of NFATc4 upon depolarization for 20 min (1.1 ± 0.14, n = 34), 60 min (2.1 ± 0.30, n = 21), or 180 min (2.5 ± 0.33, n = 22) (Fig. 9*A*). In contrast, depolarization-induced nuclear import of NFATc3 in DRG neurons was not affected by knocking down GSK3β (Fig. 9*B*). Under resting conditions, the nuclear/cytosolic ratio for EGFP-NFATc3 was 0.52 ± 0.10 for control cells (n = 30) and 0.54 ± 0.19 for DRG neurons transfected with GSK3β shRNA (n = 11) (Fig. 9*B*). Depolarization (20 mM KCl) for 20 min produced rapid and strong nuclear translocation of

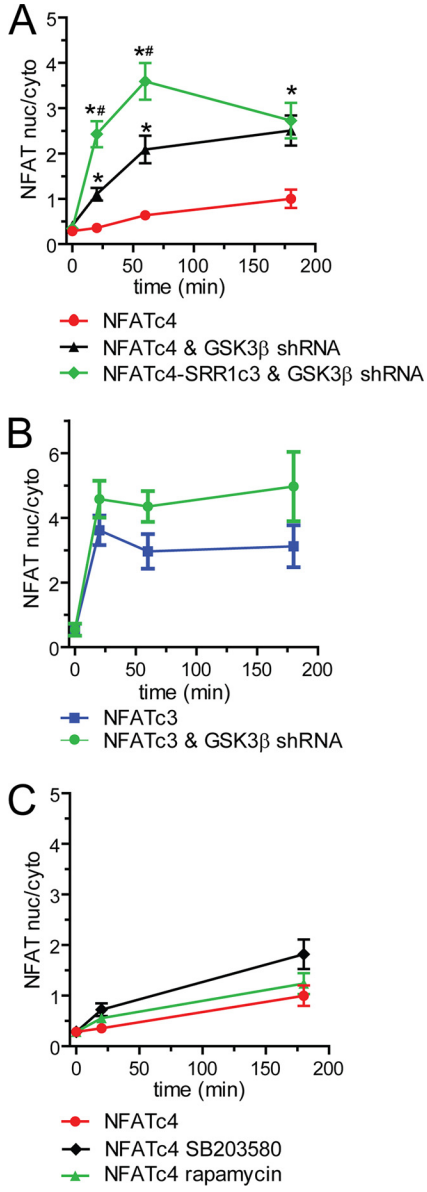

FIGURE 9. **GSK3β represses depolarization-induced nuclear translocation of NFATc4.** *A*, DRG neurons (2 DIV) transfected with EGFP-NFATc4 alone (*red circles*) or co-transfected with either EGFP-NFATc4 and GSK3β-shRNA (*black triangles*) or EGFP-NFATc4-SRRc3 and GSK3β-shRNA (*green diamonds*) were stimulated with 20 mM K^+ for 20, 60, or 180 min. Data points represent mean nuclear/cytosolic (*nuc/cyto*) fluorescence intensity ± S.E. (n = 9–34 cells). Data were compared by one-way ANOVA for each time point followed by Bonferroni post hoc test to compare constructs. *, $p < 0.05$ relative to NFATc4; #, $p < 0.05$ relative to NFATc4 + GSK3β-shRNA. *B*, DRG neurons (2 DIV) transfected with EGFP-NFATc3 alone or co-transfected with GSK3β-shRNA were stimulated with 20 mM K^+ for 20, 60, or 180 min. Data points represent mean nuclear/cytosolic fluorescence intensity ± S.E. (n = 11–27). Data were compared by one-way ANOVA for each time point followed by Bonferroni post hoc test to compare constructs. *C*, DRG neurons (1 DIV) transfected with EGFP-NFATc4 were treated with 20 mM K^+ alone (*red circles*) or together with either SB203580 (1 μM; *black diamonds*) or rapamycin (100 nM; *green triangles*) for 20 or 180 min. Data points represent mean nuclear/cytosolic fluorescence intensity ± S.E. (n = 13–40 cells).

NFATc3 yielding the EGFP-NFATc3 nuclear/cytosolic ratio of 3.6 ± 0.46 for control cells (n = 26) and 4.6 ± 0.58 for neurons treated with shRNA against GSK3β (n = 27; p = 0.20, unpaired Student's t test) (Fig. 9*B*).

The N-terminal half of the NFATc4 NHR, which contains the SRR1, also appears to inhibit NFATc4 translocation (Fig. 7, *B* and *C*). We hypothesized that replacement of the N-terminal half of the NFATc4 NHR with that of the NFATc3 NHR, which increased NFATc4 nuclear translocation at 20 and 60 min (Fig. 7*B*), would further facilitate NFATc4 nuclear translocation. Co-expression with GSK3β-shRNA had no effect on the nuclear localization of EGFP-NFATc4-SRRc3 at resting conditions that was excluded from the nucleus (0.34 ± 0.02, n = 19) (Fig. 9*A*). Following a 20-min (2.4 ± 0.29, n = 21) or 60-min (3.6 ± 0.41, n = 17) depolarization, the mean nuclear/cytosolic ratio of EGFP-NFATc4-SRRc3 in the presence of GSK3β-shRNA was significantly greater than that of EGFP-NFATc4 co-expressed with GSK3β-shRNA (Fig. 9*A*).

We also tested whether inhibition of kinases that target the SRR1 of NFATc4 would also increase NFATc4 nuclear translocation in response to depolarization. Protein kinases p38 and mTOR phosphorylate the SRR1 of NFATc4 and regulate the subcellular distribution of NFATc4 (35, 37). We stimulated DRG neurons with 20 mM K^+ in the presence of the p38 inhibitor, SB203580 (1 μM), or the mTOR inhibitor, rapamycin (100 nM), for 20 or 180 min. Neither SB203580 nor rapamycin had a significant effect on depolarization-induced nuclear translocation of NFATc4 (Fig. 9*C*). These data indicate that nuclear translocation of NFATc4 in neurons is strongly repressed by GSK3β but not by p38 or mTOR kinases.

DISCUSSION

Activity-dependent gene regulation is critical for cellular adaptations to changing environments. Neurons couple activity-driven changes in $[Ca^{2+}]_i$ to gene transcription through regulation of Ca^{2+}-dependent transcription factors, such as NFAT. There is growing evidence for the roles of particular NFAT isoforms in specific neuronal functions such as axonal and dendritic growth, synaptogenesis, sensory function, and neuronal survival (20, 21, 23, 40, 49, 51). However, whether NFAT is regulated in an isoform-specific manner in neurons is less clear. In this study, we provide evidence that NFATc3 and NFATc4 are differentially activated in response to depolarization-induced Ca^{2+} influx in DRG and hippocampal neurons, as well as in neuron-like PC12 cells. Although neuronal activity and resulting $[Ca^{2+}]_i$ elevation are sufficient to rapidly and strongly activate NFATc3 in peripheral and central neurons, NFATc4 activation requires coincident $[Ca^{2+}]_i$ elevation and repression of GSK3β. Nuclear translocation analysis of various NFATc3/c4 chimera constructs suggests that the distinct activation properties of both isoforms are determined primarily by the differences in their SP-containing regions.

Several groups have previously reported NFATc4 activation in neurons. For example, activation of L-type calcium channels by elevating extracellular K^+ (90 mM KCl) resulted in a modest CaN-dependent NFATc4 nuclear translocation in hippocampal neurons (5, 6). Stimulation of cortical neurons with NMDA induced NFATc3 and NFATc4 nuclear translocation, although the time course of translocation was not examined (21). Treatment of hippocampal neurons with brain-derived neurotrophic factor also induced NFATc4 nuclear translocation that was independent of VGCC activity (47). Importantly, the rate and amplitude of NFATc4 nuclear translocation were not compared with that of other NFAT isoforms in these studies.

Although we did observe a gradual EGFP-NFATc4 translocation in response to extended depolarization with 20 or 40 mM K^+ (Fig. 2, *B* and *C*), the responsiveness of NFATc4 was both qualitatively and quantitatively distinct from that of NFATc3.

It is increasingly apparent that cells are able to selectively activate specific NFAT isoforms, although the mechanistic basis for NFAT isoform selectivity is as yet poorly understood. In skeletal muscle cells NFATc1, NFATc2, or NFATc3 were selectively activated upon $[Ca^{2+}]_i$ elevation depending upon the stage of muscle differentiation (44). Another study in skeletal muscle found NFATc4 was constitutively localized to the nucleus, in contrast to the basal cytosolic localization of NFATc1–c3 (66). Furthermore, NFATc3 was activated by either slow or fast electrical stimulation patterns, although NFATc1 was activated only by slow patterned stimulation (66). Under basal conditions in cardiac myocytes, NFATc1 was localized to the nucleus, although NFATc3 was localized to the cytosol, and angiotensin-II and endothelin-1 stimulation induced NFATc3 nuclear translocation in atrial but not ventricular cardiac myocytes (42). Our finding that NFATc3, but not NFATc4, rapidly translocates to the nucleus of DRG and hippocampal neurons upon action potential stimulation supports the hypothesis that specific NFAT isoforms can be differentially activated within a single cell, which could contribute to NFAT isoform-specific gene regulation.

The analysis of electrophoretic mobility of NFAT isoforms suggests that NFATc3 is rapidly and effectively dephosphorylated by CaN in response to depolarization, whereas NFATc4 remains largely phosphorylated (Fig. 5*D*). This differential regulation of NFATc3 and NFATc4 by depolarization and resulting $[Ca^{2+}]_i$ elevation could be explained by distinct sensitivity of these isoforms either to dephosphorylation by CaN or to phosphorylation by NFAT kinases. The latter explanation is more attractive for two reasons. First, knocking down GSK3β markedly enhanced depolarization-induced nuclear translocation of NFATc4 (Fig. 9*A*) but not nuclear translocation of NFATc3 (Fig. 9*B*). Second, replacing either the CaN-binding P*X*I*X*IT motif or L*X*VP motif of NFATc4 with that of NFATc3 or replacing the NFATc4 P*X*I*X*IT motif with the VIVIT sequence, which binds CaN with high affinity, had little effect on depolarization-induced nuclear translocation of NFATc4 (Fig. 6, *B* and *C*).

It is unclear why GSK3β represses the nuclear translocation of NFATc4 but not of NFATc3. GSK3β activity is generally thought to require a "priming" phosphorylation on the substrate to be further phosphorylated by GSK3β (67). Previous reports indicate PKA and DYRK family kinases serve as priming kinases for GSK3β phosphorylation of NFAT (39–41). However, there are no reports of isoform-specific priming kinases, which could regulate the propensity of GSK3β to phosphorylate a given NFAT isoform. Scaffolding complexes are critical for imparting substrate specificity for GSK3β signaling, such as the well characterized axin·GSK3β·β-catenin complex in the Wnt signaling pathway (68). Recent studies identified noncoding RNA repressor of NFAT·multiprotein complexes that can contain GSK3β (69–71). Similarly, a scaffolding protein AKAP79/150 was shown to regulate interaction of NFATc4 with CaN (6, 72). Therefore, it is possible that isoform-specific regulation of NFAT proteins by protein kinases and CaN is achieved through the interaction with specific scaffolding complexes.

The respective contributions of the SRR1 and SP motifs to regulating NFAT activation remain an unresolved question. SRR1 phosphorylation is thought to be critical for occluding the NLS. Mutation of serine residues within the SRR1 increases the basal nuclear localization of NFAT (40, 57). Furthermore, simultaneous inhibition of CK1, which phosphorylates SRR1, and NFAT nuclear export with LMB increased the nuclear localization in the absence of stimulation (36). We observed that the region containing the SRR1 of NFATc4 was sufficient to decrease the initial translocation of NFATc3 in response to depolarization, although the converse substitution of the NFATc3 SRR1 into NFATc4 increased NFATc4 translocation. Interestingly, replacement of the SRR1-containing region had no effect on the amplitude of NFAT nuclear translocation following 180 min of stimulation (Fig. 7, *B* and *C*), suggesting that although the N-terminal half of the NHR may regulate the initial nuclear translocation, elements within the C-terminal half of the NHR, possibly the SP motifs, regulate the retention of NFAT within the nucleus. Indeed, replacement of the C-terminal half of the NFATc4 NHR with that of NFATc3 increased the nuclear localization at 180 min, although the converse substitution decreased NFATc3 nuclear localization (Fig. 8).

The observation that knockdown of GSK3β expression also increases the nuclear localization of NFATc4 following 180 min of depolarization suggests that the inhibitory effect of the NFATc4 C-terminal half of the NHR is likely due to persistent GSK3β-dependent phosphorylation of the SP motifs (Fig. 9). Mutation of serine residues within the SP motifs has no effect on the basal nuclear localization of NFAT (57). Similarly, we detected no increase in the basal nuclear localization of NFATc3 or NFATc4 in cells co-transfected with GSK3β-shRNA (Fig. 9). From our data, we cannot conclusively say whether GSK3β regulates NFATc4 nuclear import, export, or both import and export. Although previous studies have found that GSK3β affects the nuclear export of NFATc4 proteins, it is not known whether GSK3β also affects the rate of NFATc4 import (5). GSK3β localizes to both the cytoplasmic and nuclear compartments of neurons (73–77) and is known to phosphorylate cytosolic proteins, such as Tau (78, 79). Furthermore, GSK3β exists in cytosolic protein complexes that can repress NFAT activation (70). Interestingly, replacement of the NFATc4 N-terminal region with that of NFATc3 augmented the nuclear translocation of EGFP-NFATc4 co-expressed with GSK3β-shRNA (Fig. 9*A*). Similarly, mutation of the SP motifs augments the nuclear localization of NFAT proteins containing SRR1 mutations (40, 57). Therefore, it is likely that NFATc4 nuclear translocation in neurons is inhibited by both a strong GSK3β-dependent nuclear export and a separate repression of nuclear import regulated by dephosphorylation of SRR1.

The requirement for both electrical activity and GSK3β repression for NFATc4 activation raises the question about the endogenous mechanisms regulating GSK3β activity in neurons. One of the common signaling pathways recruited by neurotrophins involves activation of phosphatidylinositol 3-kinase (PI3K) and Akt kinase that, in turn, phosphorylates and inhibits

GSK3β (80, 81). Notably, it has been shown that NGF and brain-derived neurotrophic factor activate NFATc4 in neurons, although the specific role of the PI3K-Akt-dependent inhibition of GSK3β has not been tested in these studies (23, 48, 82).

The importance of specific NFAT proteins, in neuronal development, function, and disease, is becoming increasingly apparent. NFATc2, NFATc3, and NFATc4 regulate NGF- and netrin-dependent axonal growth during development (23). NFATc4 also regulates GAP-43 expression during development and is involved in brain-derived neurotrophic factor-dependent anti-apoptotic signaling in cortical neurons (21, 22). At the same time, NFATc3 and NFATc4 likely contribute to methamphetamine-induced neuronal apoptosis (49), and both NFATc3 and NFATc4 have been implicated in the regulation of cyclooxygenase 2 (COX-2) expression in sensory neurons (45, 82). Furthermore, recent studies have linked NFAT with neurodegeneration in Alzheimer disease, and NFATc4 activation was associated with amyloid-β-induced dendritic simplification and synapse loss in cortical neurons (24, 27, 50). Our work demonstrates that NFATc3 and NFATc4 are distinctly regulated by electrical activity and GSK3β in neurons and identifies critical regions of NFAT determining this difference. Therapeutic targeting of NFAT is currently limited by the poor specificity and associated toxicity of available compounds (60). Determination of the precise mechanisms governing activation of specific NFAT isoforms beyond CaN-dependent dephosphorylation could facilitate the discovery of novel therapeutic targets for isoform-specific NFAT modulation.

Acknowledgment—We thank Dr. Michal Hetman for the HA-NFATc4, NFATc3-shRNA, NFATc4-shRNA, and GSK3β-shRNA expression constructs.

REFERENCES

1. Cohen, S., and Greenberg, M. E. (2008) Communication between the synapse and the nucleus in neuronal development, plasticity, and disease. *Annu. Rev. Cell Dev. Biol.* **24,** 183–209
2. Dolmetsch, R. (2003) Excitation-transcription coupling: Signaling by ion channels to the nucleus. *Sci. STKE* 2003, PE4
3. Bito, H., Deisseroth, K., and Tsien, R. W. (1996) CREB phosphorylation and dephosphorylation. A Ca^{2+}- and stimulus duration-dependent switch for hippocampal gene expression. *Cell* **87,** 1203–1214
4. Deisseroth, K., Heist, E. K., and Tsien, R. W. (1998) Translocation of calmodulin to the nucleus supports CREB phosphorylation in hippocampal neurons. *Nature* **392,** 198–202
5. Graef, I. A., Mermelstein, P. G., Stankunas, K., Neilson, J. R., Deisseroth, K., Tsien, R. W., and Crabtree, G. R. (1999) L-type calcium channels and GSK-3 regulate the activity of NF-ATc4 in hippocampal neurons. *Nature* **401,** 703–708
6. Oliveria, S. F., Dell'Acqua, M. L., and Sather, W. A. (2007) AKAP79/150 anchoring of calcineurin controls neuronal L-type Ca^{2+} channel activity and nuclear signaling. *Neuron* **55,** 261–275
7. Shaw, J. P., Utz, P. J., Durand, D. B., Toole, J. J., Emmel, E. A., and Crabtree, G. R. (1988) Identification of a putative regulator of early T cell activation genes. *Science* **241,** 202–205
8. McCaffrey, P. G., Luo, C., Kerppola, T. K., Jain, J., Badalian, T. M., Ho, A. M., Burgeon, E., Lane, W. S., Lambert, J. N., Curran, T., *et al.* (1993) Isolation of the cyclosporin-sensitive T cell transcription factor NFATp. *Science* **262,** 750–754
9. Northrop, J. P., Ho, S. N., Chen, L., Thomas, D. J., Timmerman, L. A., Nolan, G. P., Admon, A., and Crabtree, G. R. (1994) NF-AT components define a family of transcription factors targeted in T-cell activation. *Nature* **369,** 497–502
10. Horsley, V., and Pavlath, G. K. (2002) NFAT. Ubiquitous regulator of cell differentiation and adaptation. *J. Cell Biol.* **156,** 771–774
11. Wu, H., Peisley, A., Graef, I. A., and Crabtree, G. R. (2007) NFAT signaling and the invention of vertebrates. *Trends Cell Biol.* **17,** 251–260
12. Molkentin, J. D., Lu, J. R., Antos, C. L., Markham, B., Richardson, J., Robbins, J., Grant, S. R., and Olson, E. N. (1998) A calcineurin-dependent transcriptional pathway for cardiac hypertrophy. *Cell* **93,** 215–228
13. Hogan, P. G., Chen, L., Nardone, J., and Rao, A. (2003) Transcriptional regulation by calcium, calcineurin, and NFAT. *Genes Dev.* **17,** 2205–2232
14. Santana, L. F. (2008) NFAT-dependent excitation-transcription coupling in heart. *Circ. Res.* **103,** 681–683
15. Graef, I. A., Chen, F., Chen, L., Kuo, A., and Crabtree, G. R. (2001) Signals transduced by Ca^{2+}/calcineurin and NFATc3/c4 pattern the developing vasculature. *Cell* **105,** 863–875
16. Bushdid, P. B., Osinska, H., Waclaw, R. R., Molkentin, J. D., and Yutzey, K. E. (2003) NFATc3 and NFATc4 are required for cardiac development and mitochondrial function. *Circ. Res.* **92,** 1305–1313
17. Rossow, C. F., Minami, E., Chase, E. G., Murry, C. E., and Santana, L. F. (2004) NFATc3-induced reductions in voltage-gated K^+ currents after myocardial infarction. *Circ. Res.* **94,** 1340–1350
18. Layne, J. J., Werner, M. E., Hill-Eubanks, D. C., and Nelson, M. T. (2008) NFATc3 regulates BK channel function in murine urinary bladder smooth muscle. *Am. J. Physiol. Cell Physiol.* **295,** C611–C623
19. Nieves-Cintrón, M., Amberg, G. C., Nichols, C. B., Molkentin, J. D., and Santana, L. F. (2007) Activation of NFATc3 down-regulates the β1 subunit of large conductance, calcium-activated K^+ channels in arterial smooth muscle and contributes to hypertension. *J. Biol. Chem.* **282,** 3231–3240
20. Benedito, A. B., Lehtinen, M., Massol, R., Lopes, U. G., Kirchhausen, T., Rao, A., and Bonni, A. (2005) The transcription factor NFAT3 mediates neuronal survival. *J. Biol. Chem.* **280,** 2818–2825
21. Vashishta, A., Habas, A., Pruunsild, P., Zheng, J. J., Timmusk, T., and Hetman, M. (2009) Nuclear factor of activated T-cells isoform c4 (NFATc4/NFAT3) as a mediator of antiapoptotic transcription in NMDA receptor-stimulated cortical neurons. *J. Neurosci.* **29,** 15331–15340
22. Nguyen, T., Lindner, R., Tedeschi, A., Forsberg, K., Green, A., Wuttke, A., Gaub, P., and Di Giovanni, S. (2009) NFAT-3 is a transcriptional repressor of the growth-associated protein 43 during neuronal maturation. *J. Biol. Chem.* **284,** 18816–18823
23. Graef, I. A., Wang, F., Charron, F., Chen, L., Neilson, J., Tessier-Lavigne, M., and Crabtree, G. R. (2003) Neurotrophins and netrins require calcineurin/NFAT signaling to stimulate outgrowth of embryonic axons. *Cell* **113,** 657–670
24. Abdul, H. M., Sama, M. A., Furman, J. L., Mathis, D. M., Beckett, T. L., Weidner, A. M., Patel, E. S., Baig, I., Murphy, M. P., LeVine, H., 3rd, Kraner, S. D., and Norris, C. M. (2009) Cognitive decline in Alzheimer disease is associated with selective changes in calcineurin/NFAT signaling. *J. Neurosci.* **29,** 12957–12969
25. Schwartz, N., Schohl, A., and Ruthazer, E. S. (2009) Neural activity regulates synaptic properties and dendritic structure *in vivo* through calcineurin/NFAT signaling. *Neuron* **62,** 655–669
26. Nguyen, T., and Di Giovanni, S. (2008) NFAT signaling in neural development and axon growth. *Int. J. Dev. Neurosci.* **26,** 141–145
27. Hudry, E., Wu, H. Y., Arbel-Ornath, M., Hashimoto, T., Matsouaka, R., Fan, Z., Spires-Jones, T. L., Betensky, R. A., Bacskai, B. J., and Hyman, B. T. (2012) Inhibition of the NFAT pathway alleviates amyloid-β neurotoxicity in a mouse model of Alzheimer disease. *J. Neurosci.* **32,** 3176–3192
28. Crabtree, G. R., and Olson, E. N. (2002) NFAT signaling. Choreographing the social lives of cells. *Cell* **109,** S67–S79
29. Macian, F. (2005) NFAT proteins. Key regulators of T-cell development and function. *Nat. Rev. Immunol.* **5,** 472–484
30. Park, S., Uesugi, M., and Verdine, G. L. (2000) A second calcineurin-binding site on the NFAT regulatory domain. *Proc. Natl. Acad. Sci. U.S.A.* **97,** 7130–7135
31. Aramburu, J., Garcia-Cózar, F., Raghavan, A., Okamura, H., Rao, A., and Hogan, P. G. (1998) Selective inhibition of NFAT activation by a peptide

spanning the calcineurin-targeting site of NFAT. *Mol. Cell* **1,** 627–637
32. Martínez-Martínez, S., Rodríguez, A., López-Maderuelo, M. D., Ortega-Pérez, I., Vázquez, J., and Redondo, J. M. (2006) Blockade of NFAT activation by the second calcineurin-binding site. *J. Biol. Chem.* **281,** 6227–6235
33. Chow, C. W., Rincón, M., Cavanagh, J., Dickens, M., and Davis, R. J. (1997) Nuclear accumulation of NFAT4 opposed by the JNK signal transduction pathway. *Science* **278,** 1638–1641
34. Gómez del Arco, P., Martínez-Martínez, S., Maldonado, J. L., Ortega-Pérez, I., and Redondo, J. M. (2000) A role for the p38 MAP kinase pathway in the nuclear shuttling of NFATp. *J. Biol. Chem.* **275,** 13872–13878
35. Yang, T. T., Xiong, Q., Enslen, H., Davis, R. J., and Chow, C. W. (2002) Phosphorylation of NFATc4 by p38 mitogen-activated protein kinases. *Mol. Cell. Biol.* **22,** 3892–3904
36. Okamura, H., Garcia-Rodriguez, C., Martinson, H., Qin, J., Virshup, D. M., and Rao, A. (2004) A conserved docking motif for CK1 binding controls the nuclear localization of NFAT1. *Mol. Cell Biol.* **24,** 4184–4195
37. Yang, T. T., Yu, R. Y., Agadir, A., Gao, G. J., Campos-Gonzalez, R., Tournier, C., and Chow, C. W. (2008) Integration of protein kinases mTOR and extracellular signal-regulated kinase 5 in regulating nucleocytoplasmic localization of NFATc4. *Mol. Cell. Biol.* **28,** 3489–3501
38. Beals, C. R., Sheridan, C. M., Turck, C. W., Gardner, P., and Crabtree, G. R. (1997) Nuclear export of NF-ATc enhanced by glycogen synthase kinase-3. *Science* **275,** 1930–1934
39. Gwack, Y., Sharma, S., Nardone, J., Tanasa, B., Iuga, A., Srikanth, S., Okamura, H., Bolton, D., Feske, S., Hogan, P. G., and Rao, A. (2006) A genome-wide *Drosophila* RNAi screen identifies DYRK family kinases as regulators of NFAT. *Nature* **441,** 646–650
40. Arron, J. R., Winslow, M. M., Polleri, A., Chang, C. P., Wu, H., Gao, X., Neilson, J. R., Chen, L., Heit, J. J., Kim, S. K., Yamasaki, N., Miyakawa, T., Francke, U., Graef, I. A., and Crabtree, G. R. (2006) NFAT dysregulation by increased dosage of DSCR1 and DYRK1A on chromosome 21. *Nature* **441,** 595–600
41. Sheridan, C. M., Heist, E. K., Beals, C. R., Crabtree, G. R., and Gardner, P. (2002) Protein kinase A negatively modulates the nuclear accumulation of NF-ATc1 by priming for subsequent phosphorylation by glycogen synthase kinase-3. *J. Biol. Chem.* **277,** 48664–48676
42. Rinne, A., Kapur, N., Molkentin, J. D., Pogwizd, S. M., Bers, D. M., Banach, K., and Blatter, L. A. (2010) Isoform- and tissue-specific regulation of the Ca^{2+}-sensitive transcription factor NFAT in cardiac myocytes and heart failure. *Am. J. Physiol. Heart Circ. Physiol.* **298,** H2001–H2009
43. Shen, T., Liu, Y., Cseresnyés, Z., Hawkins, A., Randall, W. R., and Schneider, M. F. (2006) Activity- and calcineurin-independent nuclear shuttling of NFATc1, but not NFATc3, in adult skeletal muscle fibers. *Mol. Biol. Cell* **17,** 1570–1582
44. Abbott, K. L., Friday, B. B., Thaloor, D., Murphy, T. J., and Pavlath, G. K. (1998) Activation and cellular localization of the cyclosporine A-sensitive transcription factor NF-AT in skeletal muscle cells. *Mol. Biol. Cell* **9,** 2905–2916
45. Jackson, J. G., Usachev, Y. M., and Thayer, S. A. (2007) Bradykinin-induced nuclear factor of activated T-cells-dependent transcription in rat dorsal root ganglion neurons. *Mol. Pharmacol.* **72,** 303–310
46. Kim, M. S., and Usachev, Y. M. (2009) Mitochondrial Ca^{2+} cycling facilitates activation of the transcription factor NFAT in sensory neurons. *J. Neurosci.* **29,** 12101–12114
47. Groth, R. D., and Mermelstein, P. G. (2003) Brain-derived neurotrophic factor activation of NFAT (nuclear factor of activated T-cells)-dependent transcription: a role for the transcription factor NFATc4 in neurotrophin-mediated gene expression. *J. Neurosci.* **23,** 8125–8134
48. Groth, R. D., Weick, J. P., Bradley, K. C., Luoma, J. I., Aravamudan, B., Klug, J. R., Thomas, M. J., and Mermelstein, P. G. (2008) D1 dopamine receptor activation of NFAT-mediated striatal gene expression. *Eur. J. Neurosci.* **27,** 31–42
49. Jayanthi, S., Deng, X., Ladenheim, B., McCoy, M. T., Cluster, A., Cai, N. S., and Cadet, J. L. (2005) Calcineurin/NFAT-induced up-regulation of the Fas ligand/Fas death pathway is involved in methamphetamine-induced neuronal apoptosis. *Proc. Natl. Acad. Sci. U.S.A.* **102,** 868–873
50. Wu, H. Y., Hudry, E., Hashimoto, T., Kuchibhotla, K., Rozkalne, A., Fan, Z., Spires-Jones, T., Xie, H., Arbel-Ornath, M., Grosskreutz, C. L., Bacskai, B. J., and Hyman, B. T. (2010) Amyloid β induces the morphological neurodegenerative triad of spine loss, dendritic simplification, and neuritic dystrophies through calcineurin activation. *J. Neurosci.* **30,** 2636–2649
51. Luoma, J. I., and Zirpel, L. (2008) Deafferentiation-induced activation of NFAT (nuclear factor of activated T-cells) in cochlear nucleus neurons during a developmental critical period. A role for NFATc4-dependent apoptosis in the CNS. *J. Neurosci.* **28,** 3159–3169
52. Pittman, R. N., Wang, S., DiBenedetto, A. J., and Mills, J. C. (1993) A system for characterizing cellular and molecular events in programmed neuronal cell death. *J. Neurosci.* **13,** 3669–3680
53. Ichida, M., and Finkel, T. (2001) Ras regulates NFAT3 activity in cardiac myocytes. *J. Biol. Chem.* **276,** 3524–3530
54. Tomida, T., Hirose, K., Takizawa, A., Shibasaki, F., and Iino, M. (2003) NFAT functions as a working memory of Ca^{2+} signals in decoding Ca^{2+} oscillation. *EMBO J.* **22,** 3825–3832
55. Usachev, Y. M., and Thayer, S. A. (1999) Ca^{2+} influx in resting rat sensory neurones that regulates and is regulated by ryanodine-sensitive Ca^{2+} stores. *J. Physiol.* **519,** 115–130
56. Wheeler, D. G., Barrett, C. F., Groth, R. D., Safa, P., and Tsien, R. W. (2008) CaMKII locally encodes L-type channel activity to signal to nuclear CREB in excitation-transcription coupling. *J. Cell Biol.* **183,** 849–863
57. Okamura, H., Aramburu, J., García-Rodríguez, C., Viola, J. P., Raghavan, A., Tahiliani, M., Zhang, X., Qin, J., Hogan, P. G., and Rao, A. (2000) Concerted dephosphorylation of the transcription factor NFAT1 induces a conformational switch that regulates transcriptional activity. *Mol. Cell* **6,** 539–550
58. Beals, C. R., Clipstone, N. A., Ho, S. N., and Crabtree, G. R. (1997) Nuclear localization of NF-ATc by a calcineurin-dependent, cyclosporin-sensitive intramolecular interaction. *Genes Dev.* **11,** 824–834
59. Crabtree, G. R., and Olson, E. N. (2002) NFAT signaling. Choreographing the social lives of cells. *Cell* **109,** S67–S79
60. Martínez-Martínez, S., and Redondo, J. M. (2004) Inhibitors of the calcineurin/NFAT pathway. *Curr. Med. Chem.* **11,** 997–1007
61. Liu, J., Masuda, E. S., Tsuruta, L., Arai, N., and Arai, K. (1999) Two independent calcineurin-binding regions in the N-terminal domain of murine NF-ATx1 recruit calcineurin to murine NF-ATx1. *J. Immunol.* **162,** 4755–4761
62. Zhu, J., Shibasaki, F., Price, R., Guillemot, J. C., Yano, T., Dötsch, V., Wagner, G., Ferrara, P., and McKeon, F. (1998) Intramolecular masking of nuclear import signal on NF-AT4 by casein kinase I and MEKK1. *Cell* **93,** 851–861
63. Aramburu, J., Yaffe, M. B., López-Rodríguez, C., Cantley, L. C., Hogan, P. G., and Rao, A. (1999) Affinity-driven peptide selection of an NFAT inhibitor more selective than cyclosporin A. *Science* **285,** 2129–2133
64. Müller, M. R., Sasaki, Y., Stevanovic, I., Lamperti, E. D., Ghosh, S., Sharma, S., Gelinas, C., Rossi, D. J., Pipkin, M. E., Rajewsky, K., Hogan, P. G., and Rao, A. (2009) Requirement for balanced Ca/NFAT signaling in hematopoietic and embryonic development. *Proc. Natl. Acad. Sci. U.S.A.* **106,** 7034–7039
65. Zhu, J., and McKeon, F. (1999) NF-AT activation requires suppression of Crm1-dependent export by calcineurin. *Nature* **398,** 256–260
66. Calabria, E., Ciciliot, S., Moretti, I., Garcia, M., Picard, A., Dyar, K. A., Pallafacchina, G., Tothova, J., Schiaffino, S., and Murgia, M. (2009) NFAT isoforms control activity-dependent muscle fiber type specification. *Proc. Natl. Acad. Sci. U.S.A.* **106,** 13335–13340
67. Cohen, P., and Frame, S. (2001) The renaissance of GSK3. *Nat. Rev. Mol. Cell Biol.* **2,** 769–776
68. Behrens, J., Jerchow, B. A., Würtele, M., Grimm, J., Asbrand, C., Wirtz, R., Kühl, M., Wedlich, D., and Birchmeier, W. (1998) Functional interaction of an axin homolog, conductin, with β-catenin, APC, and GSK3β. *Science* **280,** 596–599
69. Willingham, A. T., Orth, A. P., Batalov, S., Peters, E. C., Wen, B. G., Aza-Blanc, P., Hogenesch, J. B., and Schultz, P. G. (2005) A strategy for probing the function of noncoding RNAs finds a repressor of NFAT. *Science* **309,** 1570–1573
70. Sharma, S., Findlay, G. M., Bandukwala, H. S., Oberdoerffer, S., Baust, B., Li, Z., Schmidt, V., Hogan, P. G., Sacks, D. B., and Rao, A. (2011) Dephos-

phorylation of the nuclear factor of activated T cells (NFAT) transcription factor is regulated by an RNA-protein scaffold complex. *Proc. Natl. Acad. Sci. U.S.A.* **108,** 11381–11386
71. Liu, Z., Lee, J., Krummey, S., Lu, W., Cai, H., and Lenardo, M. J. (2011) The kinase LRRK2 is a regulator of the transcription factor NFAT that modulates the severity of inflammatory bowel disease. *Nat. Immunol.* **12,** 1063–1070
72. Li, H., Rao, A., and Hogan, P. G. (2004) Structural delineation of the calcineurin-NFAT interaction and its parallels to PP1 targeting interactions. *J. Mol. Biol.* **342,** 1659–1674
73. Zhou, F. Q., Zhou, J., Dedhar, S., Wu, Y. H., and Snider, W. D. (2004) NGF-induced axon growth is mediated by localized inactivation of GSK-3β and functions of the microtubule plus end binding protein APC. *Neuron* **42,** 897–912
74. Jiang, H., Guo, W., Liang, X., and Rao, Y. (2005) Both the establishment and the maintenance of neuronal polarity require active mechanisms. Critical roles of GSK-3β and its upstream regulators. *Cell* **120,** 123–135
75. Hur, E. M., and Zhou, F. Q. (2010) GSK3 signaling in neural development. *Nat. Rev. Neurosci.* **11,** 539–551
76. Gómez-Sintes, R., and Lucas, J. J. (2010) NFAT/Fas signaling mediates the neuronal apoptosis and motor side effects of GSK-3 inhibition in a mouse model of lithium therapy. *J. Clin. Invest.* **120,** 2432–2445
77. Zhou, W., Chen, L., Paul, J., Yang, S., Li, F., Sampson, K., Woodgett, J. R., Beaulieu, J. M., Gamble, K. L., and Li, X. (2012) The effects of glycogen synthase kinase-3β in serotonin neurons. *PLoS ONE* **7,** e43262
78. Jope, R. S., and Johnson, G. V. (2004) The glamour and gloom of glycogen synthase kinase-3. *Trends Biochem. Sci.* **29,** 95–102
79. Soutar, M. P., Kim, W. Y., Williamson, R., Peggie, M., Hastie, C. J., McLauchlan, H., Snider, W. D., Gordon-Weeks, P. R., and Sutherland, C. (2010) Evidence that glycogen synthase kinase-3 isoforms have distinct substrate preference in the brain. *J. Neurochem.* **115,** 974–983
80. Patapoutian, A., and Reichardt, L. F. (2001) Trk receptors. Mediators of neurotrophin action. *Curr. Opin. Neurobiol.* **11,** 272–280
81. Chao, M. V. (2003) Neurotrophins and their receptors. A convergence point for many signaling pathways. *Nat. Rev. Neurosci.* **4,** 299–309
82. Groth, R. D., Coicou, L. G., Mermelstein, P. G., and Seybold, V. S. (2007) Neurotrophin activation of NFAT-dependent transcription contributes to the regulation of pro-nociceptive genes. *J. Neurochem.* **102,** 1162–1174